

Axionlike dark-matter winds driven by galactic baryon redistribution

A.V. Nazarenko¹

Bogolyubov Institute for Theoretical Physics of NAS of Ukraine
14b, Metrolohichna Str., Kyiv 03143, Ukraine

Abstract

We examine solutions of the hydrodynamic equations for dark matter (DM) modeled as a Bose-Einstein condensate (BEC) with axionlike interaction, forming a spherically symmetric halo in dwarf galaxies. Small perturbations and decoherence of the BEC DM arise from changes in the gravitational background induced by subgalactic baryonic processes. Focusing on the events in the central region of a galaxy, overlapping with the stable DM core, we consider three scenarios: (i) expansion of a gaseous shell mimicking stellar explosions, (ii) collapse of a shell modeling star formation, and (iii) contraction of a stellar cluster toward the galactic center, driven by dynamical friction within a gaseous shell. Numerical parameters are extracted from observational data for NGC 2366. Our results show central DM density increases of 0.01 percent and DM wind velocities of up to several meters per second. A greater increase in density is observed at lower wind speeds and vice versa. These results raise the question of whether minor DM variations significantly affect star formation. In analyzing the fate of the cumulative impact of baryonic processes, we turn to the quantum excitation model with a discrete spectrum in finite volume. In the inhomogeneous DM halo, including unstable phase, metastable excitations associated with false vacuum states decay over 32 million years. This induces the decay of the system's evolutionary operator. Meanwhile, the Beliaev damping, originating from the decay of stable quasiparticles, emerges in the next order of perturbation.

1 Introduction

Axions, first introduced in quantum chromodynamics (QCD) [1], emerged as viable dark matter (DM) candidates through several foundational ideas [2–5]. In the nonrelativistic condensate, the meaning and origin of which were discussed in [6–10], axions require a transition from the QCD mass scale of $10^{-4\pm 1}$ eV/ c^2 to the ultralight regime of $10^{-22\pm 1}$ eV/ c^2 in order to form vast astronomical structures [11–20]. Meanwhile, the astrophysical treatment of dark axions inherits their chiral self-interaction [1, 21, 22], which plays a decisive role in shaping their emergent structures [22–28].

A large body of work has examined the static DM halo of dwarf galaxies modeled as a coherent Bose–Einstein condensate (BEC) of axionlike particles with various self-interactions (see, e.g., [29–32]). Certain dynamical aspects have also been addressed in [33–38]. Owing to self-interaction, BEC DM models provide a natural resolution of the central cusp problem, display a weak response to thermal perturbations while avoiding depletion, and offer greater flexibility in fitting the Lyman- α forest through additional interaction parameters, in contrast to fuzzy DM scenarios [39]. Yet, perhaps because of the complexity of comprehensive treatment, the role of BEC DM in intragalactic baryonic dynamics remains comparatively obscure.

By contrast, many results have been obtained for the interaction of DM with baryons within the frameworks of cold DM [40, 41] and warm DM [42–46], partly stimulated by the cusp problem.

Nevertheless, BEC DM at zero temperature appears to exhibit a richer spectrum of physical phenomena. This raises a natural question: how do stellar processes gravitationally influence the condensate's macroscopic wave function – both its amplitude, which determines the spatial density profile, and its phase? The magnitude of such baryonic impact depends on galaxy

¹e-mail: nazarenko@bitp.kyiv.ua

morphology and star-formation activity. In this work, we focus on DM-dominated dwarf galaxies and illustrate our approach using observational data for NGC 2366.

We employ a model for dark axions with self-interactions inherited from pioneering works [1, 21], building on earlier results in various approximations. The study of steady configurations of DM halos in NGC 2366 and its hypothetical analogues reveals a complex BEC structure composed of both stable and unstable phases, supporting liquid and gaseous states [28, 47].

Beyond the familiar Jeans gravitational instability [34, 35], which constrains the overall size of the bosonic system, there is also an internal instability due to self-interaction. This instability is signaled by the negative square of the local speed of sound, reflecting anomalous compressibility [28]. Its onset leads to fragmentation of the BEC DM, a hallmark of axion models [48, 49]. The character of this fragmentation depends on the sign of the local pressure: positive pressure favors clump formation, while negative pressure suggests a foamlike state.

These considerations naturally motivate an investigation into how such a DM model responds only to gravitational perturbations induced by baryonic processes, analyzed within the framework of hydrodynamics, where by winds we mean hydrodynamic flows. We also intend to demonstrate that the description of the fate of multiple DM perturbations requires considering quantized excitations.

2 The DM model equations

We consider the Bose–Einstein condensate (BEC) of nonrelativistic particles with mass m , described by the macroscopic complex wave function $\psi(r, t)$ of time t and radial coordinate r inside a three-dimensional ball $B(r \leq R)$. The incorporation of the axionlike self-interaction V_{int} and the potential of gravitational interaction V_{gr} leads to the Hamiltonian functional:

$$H = 4\pi \int_0^R \left[\frac{\hbar^2}{2m} |\partial_r \psi|^2 + m V_{\text{gr}} |\psi|^2 + V_{\text{int}} \right] r^2 dr, \quad (1)$$

$$V_{\text{int}} = \frac{U}{v} [1 - \cos(\sqrt{v} |\psi|)] - \frac{U}{2} |\psi|^2, \quad (2)$$

$$\Delta_r V_{\text{gr}} = 4\pi G m |\psi|^2, \quad (3)$$

where $|\psi|^2 = \psi \bar{\psi}$; $\bar{\psi}$ is the complex conjugate of ψ ; G is Newton’s constant.

The axionlike interaction (2) is chosen in analogy with [1, 21], assuming the connection between the axion field φ with the nonrelativistic wave function ψ via the relation $|\varphi|^2 = (\hbar^2/m) |\psi|^2$ [24]. Other effective axion potentials also appear in [50–53].

The self-interaction (2) is characterized by two constants, U and v , which have dimensions of energy and volume. In the particle physics [50, 52], they are related with the axion mass m and decay constant f_a as $U = mc^2$, $v = \hbar^3 c / (m f_a^2)$. Although the applicability of these relativistic relations in nonrelativistic models is controversial, they allow us to make comparisons.

The Poisson equation (3), along with its solution, is based on the radial part of the Laplace operator Δ_r and its inverse Δ_r^{-1} with respect to the variable r :

$$\Delta_r f(r) = \partial_r^2 f(r) + \frac{2}{r} \partial_r f(r), \quad (4)$$

$$\Delta_r^{-1} f(r) = -\frac{1}{r} \int_0^r f(s) s^2 ds - \int_r^R f(s) s ds. \quad (5)$$

The Gross–Pitaevskii equation is derived as

$$i\hbar \frac{\partial \psi(r, t)}{\partial t} = \frac{\delta H}{\delta \bar{\psi}(r, t)}, \quad (6)$$

taking into account the integration measure and the rules of functional differentiation for functions of the same time t :

$$\frac{\delta \psi(r', t)}{\delta \psi(r, t)} = \frac{1}{4\pi r r'} \delta(r - r'), \quad \frac{\delta \psi(r', t)}{\delta \bar{\psi}(r, t)} = 0. \quad (7)$$

We find explicitly that

$$i\hbar\partial_t\psi = -\frac{\hbar^2}{2m}\Delta_r\psi + mV_{\text{gr}}\psi + \frac{U}{2}[j_0(\sqrt{v}|\psi|) - 1]\psi, \quad (8)$$

where we refer to the spherical Bessel functions:

$$j_l(z) = z^l \left(-\frac{1}{z} \frac{d}{dz} \right)^l \frac{\sin z}{z}. \quad (9)$$

Thus, the generalized Gross–Pitaevskii equation (8) together with the Poisson equation (3) solved using (5) – GPP equations – determine the dynamics of the order parameter ψ in our model of the BEC DM.

Even if the influence of baryonic matter on DM is minimized, the ability of the coupled GPP system (8), (3) to describe real phenomena remains a challenge. The difficulties are not purely mathematical, although the equations are nonlinear. Uncertainties in the properties of DM particles prevent precise determination of the constants appearing in the equations, and the initial wave function $\psi(r)$ can be fixed only by reference to a specific physical scenario.

We intend to nondimensionalize the equations and reduce the number of free parameters to make it easier to control the solutions. Moreover, we will focus on a dwarf galaxy where DM dominates and baryon effects are weak.

Thus, we perform the replacement of model parameters $(m, U, v) \mapsto (r_0, A, f_a)$:

$$r_0 = \frac{\hbar}{\sqrt{mU}}, \quad A = \frac{8\pi G\hbar^2 m}{U^2 v}, \quad f_a = \sqrt{\frac{\hbar^3 c}{mv}}; \quad (10)$$

$$m = \left[\frac{\hbar^5 c}{8\pi G} \frac{A}{f_a^2 r_0^4} \right]^{1/4}, \quad U = \frac{\hbar^2}{mr_0^2}, \quad v = \frac{\hbar^3 c}{mf_a^2}. \quad (11)$$

The relative strength of gravitational interaction A is a dimensionless parameter, while r_0 is the distance scale, and f_a in energy units determines the decay constant of axionlike particles.

For typical orders of parameters, we obtain the mass estimate:

$$m = 0.17745 \times 10^{-22} \text{ eV } c^{-2} \left[\frac{A}{10^{-3}} \right]^{1/4} \left[\frac{r_0}{1 \text{ kpc}} \right]^{-1} \left[\frac{f_a}{10^{19} \text{ eV}} \right]^{-1/2}. \quad (12)$$

We also need the scales of time and energy:

$$t_0 = \frac{mr_0^2}{\hbar}, \quad \varepsilon_0 = \frac{\hbar^2}{2mr_0^2}. \quad (13)$$

Parametrizing the space and time variables by ξ and τ :

$$r = r_0\xi, \quad R = r_0\xi_B, \quad t = t_0\tau, \quad (14)$$

we define the dimensionless wave function:

$$\phi(\xi, \tau) = \sqrt{v} \psi(r_0\xi, t_0\tau). \quad (15)$$

We arrive at the set of dimensionless equations:

$$2i\partial_\tau\phi = -\Delta_\xi\phi + A\Phi_{\text{gr}}\phi + [j_0(|\phi|) - 1]\phi, \quad (16a)$$

$$\Phi_{\text{gr}}(\xi, \tau) = \Phi_0(\tau) + \int_0^\xi \left(\frac{1}{s} - \frac{1}{\xi} \right) |\phi(s, \tau)|^2 s^2 ds, \quad (16b)$$

where the term

$$\Phi_0(\tau) \equiv - \int_0^{\xi_B} |\phi(s, \tau)|^2 s ds \quad (17)$$

defines the gravitational potential at the origin.

Although a complex solution ϕ to equations (16) is governed by the dimensionless constant A , the physical characteristics also depend on the dimensional r_0 and f_a . Defining the amplitude χ :

$$\phi(\xi, \tau) = \chi(\xi, \tau) e^{i\theta(\xi, \tau)}, \quad (18)$$

the local DM mass density is $\rho = \rho_0 \chi^2$, where $\rho_0 \equiv m/v$, and the number of DM particles contained under a sphere of radius $\xi = r/r_0$ is determined, omitting the factor $4\pi r_0^3/v$, by the integral:

$$n(\xi, \tau) = \int_0^\xi \chi^2(s, \tau) s^2 ds; \quad \mathcal{N} \equiv n(\xi_B, \tau). \quad (19)$$

Substituting (18) into (16a) and separating the real and imaginary parts, we arrive at a pair of equations:

$$2\partial_\tau \chi + 2\partial_\xi \chi \partial_\xi \theta + \chi \Delta_\xi \theta = 0, \quad (20)$$

$$2\partial_\tau \theta + (\partial_\xi \theta)^2 - \frac{1}{\chi} \Delta_\xi \chi + W[\chi] = 0; \quad (21)$$

$$W[\chi] \equiv A\Phi_{\text{gr}} + j_0(\chi) - 1. \quad (22)$$

As shown in [28], the self-interaction $j_0(\chi)$ induces an alternation of phases: unstable for $\chi \in [a_{2n-1}; a_{2n}]$ and stable for $\chi \in [a_{2n}; a_{2n+1}]$ phases, where the sequence $\{a_n\}$ is defined by the zeros of $j_1(a_n) = 0$, with $a_1 = 0$ and $a_{n-1} < a_n$. Although infinitely many such phases exist, in practice we consider only two: an unstable one for $\chi < a_2$, and a stable one for $a_2 < \chi < a_3$.

Since the model is designed to describe the DM distribution, it must, like other self-interacting models, address the cusp problem at the origin [29, 30]. The condition $\chi'(0, \tau) = 0$, dictated by spherical symmetry, smooths the central peak. However, determining $\chi(0, \tau)$ in a nonlinear model is nontrivial and is discussed in detail in [28, 54].

Besides, we initially assume the existence of a solution within a finite spatial domain, $\xi \in [0; \xi_B]$, where the boundary value ξ_B is determined by the condition $j_0(\chi(\xi_B, \tau)) = 0$. For convenience, we set $\chi(\xi_B, \tau) = \pi$, so that the interval $\xi \in [0; \xi_B]$ encompasses both phases. The correspondence between ξ_B and dimensional R is governed by the scale r_0 . Meanwhile, the phase θ depends significantly on the chosen physical regime.

In the case of a *coherent* BEC, the DM is characterized by a fixed quantity – a constant chemical potential

$$\tilde{\mu} = \frac{\hbar^2}{mr_0^2} u, \quad (23)$$

which is parametrized by a dimensionless $u < 0$. Therefore, the phase takes on the form:

$$\theta = -\frac{\tilde{\mu}t}{\hbar} = -u\tau. \quad (24)$$

In a spherical DM model, the constancy of its chemical potential may be attributed to the uniform gravitational potential produced inside the sphere by the isotropic outer shell of surrounding matter.

Substituting (24) in (21) leads to stationary GPP equations with an effective parameter $\nu = 1 + 2u - A\Phi_0$:

$$(\Delta_\xi + \nu)\chi - A\Phi\chi - \sin \chi = 0, \quad (25a)$$

$$\Phi = \int_0^\xi \left(\frac{1}{s} - \frac{1}{\xi} \right) \chi^2(s) s^2 ds. \quad (25b)$$

Solutions and macroscopic properties of such a model have been studied previously in [28], including applications to the dwarf galaxy NGC 2366.

The case of a nonuniform phase, when $\partial_\xi\theta \neq 0$, corresponds to *decoherent* BEC DM. The dephasing of parts of the condensate can be caused by an external impact with the momentum transfer, which leads to the emergence of a DM flow with a local speed

$$v(\xi, \tau) = \partial_\xi\theta(\xi, \tau). \quad (26)$$

The symmetry of the model eliminates the vortex contribution to the velocity v , leaving us only the gradient part.

Multiplying (20) by χ and taking into account the definition of the particle number density $\eta = \chi^2$, one obtains the continuity equation for a spherical model:

$$\partial_\tau\eta + \frac{1}{\xi^2}\partial_\xi(\xi^2\eta v) = 0. \quad (27)$$

On the other hand, by differentiating (21) with respect to ξ , we arrive at the Euler hydrodynamic equation:

$$\partial_\tau v + \partial_\xi \left[\frac{v^2}{2} - \frac{1}{2\sqrt{\eta}}\Delta_\xi\sqrt{\eta} + \frac{1}{2}W[\sqrt{\eta}] \right] = 0. \quad (28)$$

In the next section, we extend these equations by including terms that account for the gravitational perturbations induced by baryonic matter. By progressively incorporating such perturbations over time, the stationary solutions of (25) serve as initial conditions. In section 4, we return to the autonomous equations to investigate the quantum aspects of DM excitations.

3 The impact of baryonic perturbations on DM

3.1 Clustering of baryonic matter. The case of dwarf NGC 2366

To capture the qualitative effects of star formation and stellar feedback on BEC DM under spherical symmetry, we intend to extract the central star/gas cluster (overdensity) as a spherical shell near the galactic center, independent of the overall shape of the galaxy. We distribute baryonic matter (stars and gas) unevenly across the radius in a spherical shell whose thickness is governed by the scale d , allowing d to contract during collapse and grow during explosive events. Although the processes that redistribute baryons are complex and omitted here, our interest lies in the consequent changes to the gravitational potential and the resulting response of DM.

We generalize the Plummer spherical profile of density [55], originally centered at the origin, to a baryonic cluster whose center is currently defined by radius-vector $\check{\mathbf{r}}$ by replacing $\mathbf{r} \rightarrow \mathbf{r} - \check{\mathbf{r}}$. To obtain a spherical shell model we then average this shifted profile over all orientations, using $s \in [-1; 1]$ (cosine of the angle between \mathbf{r} and $\check{\mathbf{r}}$), producing a normalized radial distribution that depends only on the scalar radius r :

$$\begin{aligned} \eta_b(r, \check{r}, d) &= \frac{3d^2}{2} \int_{-1}^1 \frac{ds}{(r^2 - 2r\check{r}s + \check{r}^2 + d^2)^{5/2}} \\ &= \frac{d^2}{2r\check{r}} \left[\frac{1}{[(r - \check{r})^2 + d^2]^{3/2}} - \frac{1}{[(r + \check{r})^2 + d^2]^{3/2}} \right]; \end{aligned} \quad (29)$$

$$\int_0^\infty \eta_b(r, \check{r}, d) r^2 dr = 1. \quad (30)$$

In particular, the Plummer profile is restored as

$$\lim_{\check{r} \rightarrow 0} \eta_b(r, \check{r}, d) = \frac{3d^2}{(r^2 + d^2)^{5/2}}. \quad (31)$$

Note that various aspects of shells in general relativity and astrophysics are in [56–58].

cluster	\check{r}_i [kpc]	d_i [kpc]	M_i [$10^6 M_\odot$]
1	1.10	0.23	8.042
2	1.66	0.51	38.20
3	2.52	0.64	145.8
4	3.76	0.84	202.1
5	4.84	1.24	264.7
6	6.57	1.91	189.1

Table 1: Parameters of the gas clusters.

cluster	\check{r}_i [kpc]	d_i [kpc]	M_i [$10^6 M_\odot$]
1	0.46	0.24	12.32
2	1.10	0.09	16.34
3	1.45	1.01	13.07
4	2.04	0.03	22.37
5	3.17	1.42	138.7
6	5.97	2.00	113.1

Table 2: Parameters of the star clusters.

The shell profile (29) is asymmetric, with a peak at

$$r_p \simeq \check{r} \left[1 - \frac{d^2}{3\check{r}^2} - \frac{d^4}{18\check{r}^4} + O\left(\frac{d^5}{\check{r}^5}\right) \right], \quad (32)$$

when $d < \check{r}$; and the profile decays rapidly over the scale d for the deviation $|r - r_p|$.

The total baryon mass M of such a cluster is distributed uniformly over solid angle so that $d^2M/d\Omega^2 = M/(4\pi)$, while the volumetric mass density is

$$4\pi \frac{d^3M}{r^2 dr d\Omega^2} = M \eta_b(r, \check{r}, d). \quad (33)$$

Estimating the integral

$$\int_{\check{r}-d}^{\check{r}+d} \eta_b(r, \check{r}, d) r^2 dr = \frac{\sqrt{2}}{2} - \frac{1}{8} \frac{d^3}{\check{r}^3} + O\left(\frac{d^5}{\check{r}^5}\right), \quad (34)$$

we conclude that the spherical layer $r \in [\check{r} - d, \check{r} + d]$ contains mass $\sim 0.7M$ if $d \ll \check{r}$. Then the mean mass density of the layer is estimated as

$$\bar{\rho}_b \simeq \frac{M}{16\pi} \frac{\sqrt{2}}{d\check{r}^2}. \quad (35)$$

Moreover, when dealing with observational data, we need to introduce the surface density $\Sigma_0(R, \check{r}, d)$ associated with the spatial distribution $\eta_b(r, \check{r}, d)$. Analytically, the function $\Sigma_0(R, \check{r}, d)$ is written in terms of elliptic integrals and has a complex form in appendix A. Then, by extracting the parameters of each cluster using it, we can approximately reconstruct its spatial distribution.

Here we turn to observational data on the distribution of gas (G) and stars (S) in the dwarf galaxy NGC 2366 from [59]. We approximate the surface density profiles using six clusters:

$$\Sigma(R) = \sum_{i=1}^6 \frac{M_i}{4\pi} \Sigma_0(R, \check{r}_i, d_i). \quad (36)$$

Cluster decompositions with the parameters from Tabs. 1 and 2 are shown in figure 1a and 2a. Reconstructing the model spatial distributions as

$$\rho(r) = \sum_{i=1}^6 \frac{M_i}{4\pi} \eta_b(r, \check{r}_i, d_i), \quad (37)$$

the obtained profiles are shown in figures 1b and 2b.

It should be stressed that while a spherically symmetric distribution may provide a reasonable approximation near the galactic center, it fails at the periphery where the galaxy's geometry is distinctly non-spherical.

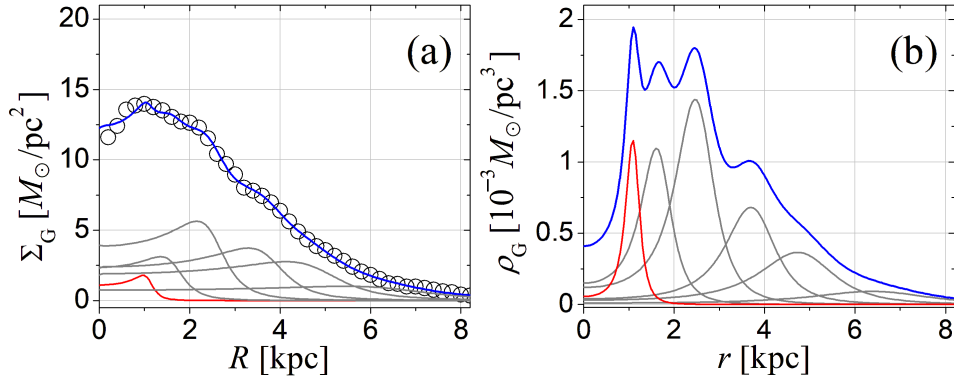


Figure 1: Interstellar gas distributions in NGC 2366. The blue curves envelope cluster contributions, colored in gray and red. Circles in panel (a) are the data from [59].

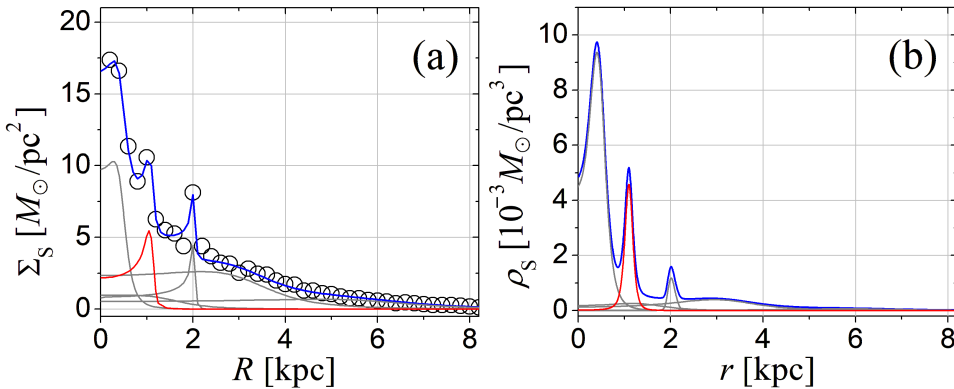


Figure 2: Stellar distributions in NGC 2366. The blue curves envelope the cluster contributions, colored in gray and red. Circles in panel (a) are the data from [59].

Analyzing the cluster data, we note that gas cluster-1 is located at $\check{r} = 1.1$ kpc, coinciding with the shell core position of star cluster-2. Both clusters are colored red in figures 1, 2. This spatial overlap may suggest either a local accumulation of gas around the stars of cluster-2 or gas ejection originating from them. Given the relatively high gas mobility, we next consider how changes in the width d_1 of its spatial distribution, arising in both scenarios, may exert gravitational influence on the surrounding DM.

The presence of star cluster-1 near the galactic center suggests an additional scenario: the possible inward approach of star cluster-2, accompanied by a decrease in \check{r}_2 . Such a motion could be caused by the migration of stars toward the galactic center, a process usually explained by dynamical friction.

These baryonic clusters, whose sphericity is allowed for $r \leq 1$ kpc, spatially overlap the dense phase of the DM core, which will experience the strongest perturbations during the hypothetical processes. According to the DM profile for NGC 2366 in [28], this phase is determined by the amplitude range $a_2 = 4.493409 < \chi < 6.551148 = \chi_0$ for $r < 2.48$ kpc.

When modeling the processes, we nondimensionalize the quantities. Since the chosen baryon distribution is a homogeneous function, we simply have

$$\eta_b(r, \check{r}, d) = r_0^{-3} \eta_b(\xi, \check{\xi}, \ell), \quad (38)$$

where

$$\xi = \frac{r}{r_0}, \quad \check{\xi} = \frac{\check{r}}{r_0}, \quad \ell = \frac{d}{r_0}. \quad (39)$$

Using $r_0 = 1.18$ kpc and $m = 0.1171 \times 10^{-22}$ eV c^{-2} for DM in NGC 2366 from [28], we

introduce the scales of velocity and time:

$$v_0 \equiv \frac{\hbar}{mr_0} \simeq 1.387451 \times 10^5 \text{ m/s}, \quad (40)$$

$$t_0 \equiv \frac{mr_0^2}{\hbar} \simeq 2.624308 \times 10^{14} \text{ s} \simeq 8.316 \times 10^6 \text{ yr}. \quad (41)$$

These scales are used in the rest of the article.

3.2 Partial gravitational potentials

According to Gauss theorem, the gravitational potential of a *thin* shell remains constant inside the shell, but outside it obeys Newton's inverse-radius law. Smoothing the shell over a finite width only softens local features and does not change the large-scale trend, making the detailed shape of $\eta_b(\xi, \check{\xi}, \ell)$ irrelevant. The use of the modified Plummer profile merely simplifies the analytical description.

Based on these ideas, the Poisson equation $\Delta_\xi \Phi_b = \eta_b(\xi, \check{\xi}, \ell)$, with Δ_ξ the radial part of the Laplacian, yields the potential:

$$\Phi_b(\xi, \check{\xi}, \ell) = -\frac{\sqrt{(\xi + \check{\xi})^2 + \ell^2} - \sqrt{(\xi - \check{\xi})^2 + \ell^2}}{2\xi\check{\xi}}; \quad (42)$$

$$\Phi_b(\xi, 0, \ell) = -\frac{1}{\sqrt{\xi^2 + \ell^2}}. \quad (43)$$

The value $\Phi_b(0, \check{\xi}, \ell)$ is obtained from the last expression by interchanging ξ and $\check{\xi}$.

Then the total gravitational potential created by all baryonic clusters is equal to

$$V_b(\xi) = \sum_{k \in \text{all clusters}} A_b^{(k)} \Phi_b\left(\xi, \frac{\check{r}_k}{r_0}, \frac{d_k}{r_0}\right), \quad (44)$$

where $A_b^{(k)}$ is the dimensionless coupling for baryonic cluster- k with the total mass M_k :

$$A_b^{(k)} = 2 \frac{GM_k m^2 r_0}{\hbar^2}. \quad (45)$$

Substituting the parameters of NGC 2366's DM, one estimates, in general,

$$A_b \simeq 3.80 \times 10^{-4} \left[\frac{M}{10^6 M_\odot} \right]. \quad (46)$$

By perturbing the coherent BEC DM with the gravitational influence of redistributing baryonic matter, we require the presence in (25) of an initial gravitational background created by baryons. However, it is absorbed by the parameter u defined in (23), when the DM dominates, as

$$2u = 2u_0 + \langle V_b \rangle. \quad (47)$$

Here the second term represents the quantum mean of the gravitational potential and corresponds to the first correction of perturbation theory, the mean field:

$$\langle V_b \rangle = \langle \phi | V_b | \phi \rangle = \frac{1}{\mathcal{N}} \int_0^{\xi_B} V_b(s) \chi^2(s) s^2 ds, \quad (48)$$

see (18) and (19) for using unnormalized ϕ .

By reproducing the rotation curve for NGC 2366 in [28], the equilibrium DM distribution $\eta(\xi) \equiv \chi^2(\xi)$ in figure 4a below is obtained for the constant chemical potential $2u = -1.5867$. Using this fact and substituting the cluster parameters from table 1 and 2, we calculate that

$\langle V_b \rangle = -0.0926$ and, accordingly, $2u_0 = -1.4941$. This confirms the approximation (47) and may indicate an external source for the main contribution, $2u_0$.

Although the potential V_b includes contributions from all feasible clusters, we intend to analyze the impact caused by restructuring a single cluster, avoiding the DM condensate depletion. By synchronously redistributing the baryons in the selected cluster, we obtain a new gravitational potential:

$$V'_b = V_b + A_b \Delta \Phi_b, \quad (49)$$

where $\Delta \Phi_b$ denotes the change in the gravitational potential, defined as the final potential minus the initial potential.

We assume mass conservation for the cluster: its total mass M remains fixed while the cluster's profile/position may vary. Given (47), the perturbed baryonic contribution acting on the DM, to the same order of approximation, becomes

$$\langle V_b \rangle \rightarrow \langle V_b \rangle + A_b \Delta \Phi_b. \quad (50)$$

Such changes occur adiabatically:

$$\left| \frac{\Delta \Phi_b}{\Phi_b} \right| \ll 1. \quad (51)$$

Since $A_b |\Delta \Phi_b| \ll |V_b|$, the perturbation produces only a negligible change in the DM density profile. The condensate, however, does acquire a spatially varying phase. This induced phase inhomogeneity drives decoherence of the condensate and generates macroscopic flows.

With small changes in the geometric parameters of the baryon distribution, we can write:

$$\delta \Phi_b(\xi, \check{\xi}, \ell) = \Phi_\ell(\xi, \check{\xi}, \ell) \delta \ell + \Phi_\xi(\xi, \check{\xi}, \ell) \delta \check{\xi}. \quad (52)$$

where $\Phi_\ell \equiv \partial \Phi_b / \partial \ell$ and $\Phi_\xi \equiv \partial \Phi_b / \partial \check{\xi}$.

Formula (52) indicates two types of possible processes associated either with the matter redistribution in the shell or with a displacement of the entire shell. Moreover, it provides a basis for variable separation, allowing the potential change to be expressed as $\delta \Phi_b = \Phi_x(\xi) \delta x(\tau)$.

We easily find that

$$\Phi_\ell(\xi, \check{\xi}, \ell) = \frac{\ell}{2\check{\xi}\xi} \left[\frac{1}{J_-(\xi, \check{\xi}, \ell)} - \frac{1}{J_+(\xi, \check{\xi}, \ell)} \right], \quad (53)$$

$$\Phi_\xi(\xi, \check{\xi}, \ell) = -\frac{1}{2\check{\xi}^2\xi} \left[\frac{\xi^2 - \xi\check{\xi} + \ell^2}{J_-(\xi, \check{\xi}, \ell)} - \frac{\xi^2 + \xi\check{\xi} + \ell^2}{J_+(\xi, \check{\xi}, \ell)} \right], \quad (54)$$

where

$$J_\pm(\xi, \check{\xi}, \ell) \equiv \sqrt{(\xi \pm \check{\xi})^2 + \ell^2}. \quad (55)$$

Assuming that the time dependence is concentrated in $\delta x(\tau)$, we adopt the relaxation-time approximation for all processes, thereby unifying our approach:

$$\frac{d^2 \delta x}{d\tau^2} + \frac{1}{\tau_{ch}} \frac{d\delta x}{d\tau} = 0, \quad \delta x(0) = 0, \quad \delta x(\tau) \xrightarrow{\tau \rightarrow \infty} \delta x_\infty, \quad (56)$$

where τ_{ch} is the characteristic relaxation time; and δx_∞ is the asymptotic (final) value.

It means that the velocity $\delta \dot{x}(\tau)$ decays over time, driven either by a counteracting force or by saturation effects. Such a solution is given by the expression:

$$\delta x(\tau) = \delta x_\infty (1 - e^{-\gamma\tau}), \quad \gamma \equiv \frac{1}{\tau_{ch}}. \quad (57)$$

Thus, $\delta \Phi_b = \Phi_\ell(\xi, \check{\xi}, \ell) \delta \ell$ provides a linear approximation to the difference $\Delta \Phi_b = \Phi_b(\xi, \check{\xi}, \ell + \delta \ell) - \Phi_b(\xi, \check{\xi}, \ell)$, which arises from a temporal variation of $\delta \ell(\tau)$. The case of $\check{\xi} = 0.932$, $\ell = 0.195$,

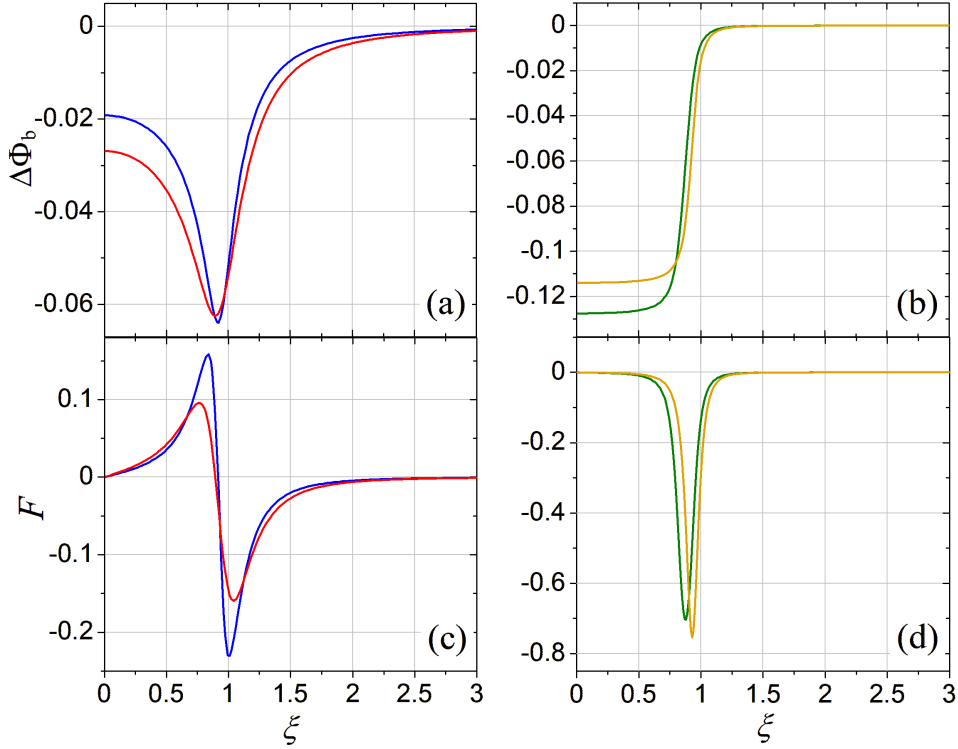


Figure 3: Top row: gravitational potential differences $\Delta\Phi_b$ (blue and green) and potential variations $\delta\Phi_b$ (red and orange). Panel (a): changes induced by narrowing the width ℓ at fixed position $\check{\xi}$. Panel (b): changes caused by a small leftward shift of $\check{\xi}$ at fixed ℓ . Bottom row: corresponding forces F , given by $-\partial_\xi\Delta\Phi_b$ and $-\partial_\xi\delta\Phi_b$, displayed in the same colors as their associated potential changes.

and the final $\delta\ell_\infty = -0.119$, used below, is shown in figure 3a. A change in gravitational potential results in the emergence of a force, determined by

$$-\partial_\xi\Phi_\ell(\xi, \check{\xi}, \ell) = \frac{\ell}{2\check{\xi}\xi^2} \left[\frac{1}{J_-(\xi, \check{\xi}, \ell)} - \frac{1}{J_+(\xi, \check{\xi}, \ell)} \right] + \frac{\ell}{2\check{\xi}\xi} \left[\frac{\xi - \check{\xi}}{J_-^3(\xi, \check{\xi}, \ell)} - \frac{\xi + \check{\xi}}{J_+^3(\xi, \check{\xi}, \ell)} \right]. \quad (58)$$

The dependence of this force on time is also given by the factor $\delta\ell(\tau)$ for some τ_{ch} .

Under the specified parameters, the collapse-induced compression of baryonic matter from $\ell = 0.195$ to $\ell = 0.076$ yields the force profile presented in figure 3c. Conversely, by reversing the force direction and changing its sign, one can evaluate the force acting on DM, for instance, during expansion or explosion. It is essential, however, to account for the varying influences that arise from different process rates γ .

Another special case, $\delta\Phi_b = \Phi_\xi(\xi, \check{\xi}, \ell)\delta\check{\xi}$, corresponds to a potential change $\Delta\Phi_b = \Phi_b(\xi, \check{\xi} + \delta\check{\xi}, \ell) - \Phi_b(\xi, \check{\xi}, \ell)$, arising from a cluster shift driven by the time-dependent variation $\delta\check{\xi}(\tau)$. For $\check{\xi} = 0.932$, $\ell = 0.076$, and the final value $\delta\check{\xi}_\infty = -0.1$, the resulting profiles are shown in figure 3b. The corresponding force can then be estimated using the expression:

$$-\partial_\xi\Phi_\xi(\xi, \check{\xi}, \ell) = -\frac{\ell^2}{2\check{\xi}^2\xi^2} \left[\frac{1}{J_-(\xi, \check{\xi}, \ell)} - \frac{1}{J_+(\xi, \check{\xi}, \ell)} \right] + \frac{\ell^2}{2\check{\xi}\xi} \left[\frac{1}{J_-^3(\xi, \check{\xi}, \ell)} + \frac{1}{J_+^3(\xi, \check{\xi}, \ell)} \right]. \quad (59)$$

Although the contraction of an entire cluster toward the galactic center occurs gradually, figure 3d demonstrates that the exerted force is substantial. We therefore turn to examining the impact of cluster migration on DM.

3.3 Migration rate of a star cluster under dynamical friction

Although a rough estimate of τ_{ch} or γ is sufficient, in principle, to account for the gravitational influence of star-cluster migration on DM, we now examine the migration process in greater detail. In our modeling, we focus on the extracted shell-like star cluster-2, embedded within the wider gas cluster-1 of NGC 2366. Under these conditions, studying the dynamical friction mechanism, which has traditionally been analyzed for a pointlike perturber after Chandrasekhar's work [60], becomes particularly relevant.

Let us isolate from the spherical star cluster-2 a toroidal tube (ring) with a cross-sectional diameter of $2d_{sc}$, lying on the equator with $r = \check{r}$. According to (35), the mean mass density of the star cluster-2 is $\bar{\rho}_{sc} \simeq 2.877 \times 10^{-22} \text{ kg/m}^3$ at $M_{sc} \simeq 16.34 \times 10^6 M_{\odot}$, and the tube's volume is $v_{tube} = 2\pi^2 \check{r} d_{sc}^2 \simeq 0.176 \text{ kpc}^3$, which gives us its mass $\mu = \bar{\rho}_{sc} v_{tube} \simeq 7.42 \times 10^5 M_{\odot}$.

Then the spherical cluster is covered by a number of $N = M_{sc}/\mu \simeq 22.01$ tubes, each of which has a moment of inertia $I = \mu \check{r}^2$ at $d_{sc} \ll \check{r}$ and its own axis of rotation with the same angular frequency $\Omega(\check{r})$ determined by the rotation curve of the galaxy.

The total kinetic energy of the star cluster is

$$K_{sc} = N \frac{I \Omega^2(\check{r})}{2} = \frac{M_{sc} V_t^2(\check{r})}{2}, \quad (60)$$

where the tangential velocity $V_t(\check{r}) = \check{r} \Omega(\check{r})$. Here, $V_t \simeq 22 \text{ km/s}$, as inferred from the rotation curve in [28], which allows us to consider the effect in the supersonic regime.

Thus, for simplicity, we densely cover a sphere of radius $r = \check{r}$ with stars rotating along circular equatorial orbits and collectively producing the gravitational potential of a sphere:

$$W_{sc}(r) = -\frac{GM_{sc}}{\check{r}} H(\check{r} - r) - \frac{GM_{sc}}{r} H(r - \check{r}), \quad (61)$$

where the Heaviside function $H(r)$ is used.

On the other hand, we take into account the spatial distribution of the mass $\rho_{gc}(r, \check{r}, d_{gc})$ in gas cluster-1, which generates the gravitational potential $GM_{gc}\Phi(r, \check{r}, d_{gc})$.

The change in the kinetic energy of the star cluster over time is written as

$$\dot{K}_{sc} = M_{sc} V_t \dot{V}_t = -\frac{2\alpha}{t_{df}} K_{sc}, \quad (62)$$

where we define the rate and the slope:

$$\frac{1}{t_{df}} \equiv -\frac{\dot{\check{r}}}{\check{r}} > 0, \quad \alpha = \left. \frac{d \ln V_t(r)}{d \ln r} \right|_{r=\check{r}}. \quad (63)$$

We obtain that $\alpha \simeq 0.94$ from the data in [28].

Therefore, one finds that

$$\frac{\alpha}{t_{df}} = \left| \frac{\dot{K}_{sc}}{2K_{sc}} \right| = \left| \frac{\dot{V}_t}{V_t} \right|. \quad (64)$$

Assuming that the change in the kinetic energy of the star cluster is caused by a change in the gravitational potential of the gas wake W_w , we set

$$\left| \frac{\dot{K}_{sc}}{2K_{sc}} \right| = \left| \frac{\dot{W}_w}{V_t^2} \right|. \quad (65)$$

To find \dot{W}_w , we allow a redistribution of the gas mass driven by gravitational focusing near the surface $r = \check{r}$:

$$\dot{m}_{gc}(r, \check{r}, d_{gc}) = u(r) \frac{\partial}{\partial d_{gc}} m_{gc}(r, \check{r}, d_{gc}), \quad (66)$$

where $u(r)$ is a radial velocity of cluster compression; the mass under a sphere of radius r

$$m_{\text{gc}}(r, \check{r}, d_{\text{gc}}) = 4\pi \int_0^r \rho_{\text{gc}}(s, \check{r}, d_{\text{gc}}) s^2 ds, \quad m_{\text{gc}}(\infty, \check{r}, d_{\text{gc}}) = M_{\text{gc}}. \quad (67)$$

Differentiating (66) with respect to r , we arrive at the continuity equation:

$$\partial_t \rho_{\text{gc}} + \frac{1}{r^2} \partial_r (r^2 \rho_{\text{gc}} v) = 0, \quad (68)$$

$$v = -\frac{u(r)}{\rho_{\text{gc}}(r, \check{r}, d_{\text{gc}})} \frac{\partial}{\partial d_{\text{gc}}} \frac{m_{\text{gc}}(r, \check{r}, d_{\text{gc}})}{r^2}. \quad (69)$$

The time derivative of the excess gravitational force F_w per unit probe mass acting on the stars at $t = 0$ is equal to

$$\dot{F}_w = Gu(r) \frac{\partial}{\partial d_{\text{gc}}} \frac{m_{\text{gc}}(r, \check{r}, d_{\text{gc}})}{r^2} = -GM_{\text{gc}} u(r) \frac{\partial^2}{\partial r \partial d_{\text{gc}}} \Phi(r, \check{r}, d_{\text{gc}}). \quad (70)$$

By relating the specific force F_w to W_w , one has

$$\dot{W}_w = -\int_0^\infty \dot{F}_w dr = -GM_{\text{gc}} \int_0^\infty \frac{\partial}{\partial d_{\text{gc}}} \Phi(r, \check{r}, d_{\text{gc}}) du(r), \quad (71)$$

where we neglect the boundary terms by performing integration by parts.

Having defined the infinitesimal velocity $du(r) = -\partial_r W_{\text{sc}} dt$ according to the Newton equation, we can write that

$$\dot{W}_w = -GM_{\text{gc}} \int_0^\infty dT(r) \left(-\frac{dW_{\text{sc}}(r)}{dr} \right) \frac{\partial}{\partial d_{\text{gc}}} \Phi(r, \check{r}, d_{\text{gc}}) \quad (72)$$

where $T(r) = 2\pi r/V_t(r) \simeq 2\pi r/V_t(\check{r})$ and $dT(r) \simeq 2\pi dr/V_t(\check{r})$, since the integrand is sharply peaked within a narrow radial interval.

Computing the integral by using (53) and dimensionless variables, one gets

$$\int_{\check{\xi}}^\infty \Phi_\ell(\xi, \check{\xi}, \ell) \frac{d\xi}{\xi^2} = \frac{\ell}{4} \frac{2\check{\xi}^2 - \ell^2}{\check{\xi} (\check{\xi}^2 + \ell^2)^{5/2}} \left[2 \operatorname{arctanh} \frac{\check{\xi}}{\sqrt{\check{\xi}^2 + \ell^2}} - \operatorname{arctanh} \frac{2\check{\xi}^2 + \ell^2}{\sqrt{\check{\xi}^2 + \ell^2} \sqrt{4\check{\xi}^2 + \ell^2}} \right. \\ \left. + \operatorname{arctanh} \frac{\ell}{\sqrt{\check{\xi}^2 + \ell^2}} \right] + \frac{\ell}{4} \frac{\ell^3 + 4\check{\xi}^2 \ell - 6\check{\xi}^3 + (2\check{\xi}^2 - \ell^2) \sqrt{4\check{\xi}^2 + \ell^2}}{\check{\xi}^3 (\check{\xi}^2 + \ell^2)^2}.$$

Evaluating this Coulomb-type integral for the parameters $\check{\xi} \gg 1$ and $\ell \ll \check{\xi}$ leads to

$$\int_{\check{\xi}}^\infty \Phi_\ell(\xi, \check{\xi}, \ell) \frac{d\xi}{\xi^2} \simeq \frac{\ell}{2\check{\xi}^4} \ln \frac{\check{\xi}}{\ell}. \quad (73)$$

Using the mean gas density (35) and combining the formulas, we derive

$$\dot{W}_w = 16\sqrt{2}\pi^2 \frac{G^2 M_{\text{sc}} \bar{\rho}_{\text{gc}}}{V_t} \left(\frac{d_{\text{gc}}}{\check{r}} \right)^2 \ln \frac{\check{r}}{d_{\text{gc}}}. \quad (74)$$

Therefore, the initial rate of dynamical friction is given by

$$\frac{1}{t_{\text{df}}} \simeq 16\sqrt{2}\pi^2 \frac{G^2 M_{\text{sc}} \bar{\rho}_{\text{gc}}}{\alpha V_t^3} \left(\frac{d_{\text{gc}}}{\check{r}} \right)^2 \ln \frac{\check{r}}{d_{\text{gc}}}. \quad (75)$$

This expression differs from many other relaxation time estimates for linear [60–63] and circular [64–67] motions of perturber even in the supersonic regime, in a geometrical factor that indicates

a peculiarity of our two-spherical-shell model. When the gas environment is replaced by DM from different models [68–72], differences are also revealed. However, the scale of dynamic friction for stars in a gaseous medium may be compared for different geometries.

Thus, substituting the cluster parameters and $\bar{\rho}_{\text{gc}} \simeq 5.5 \times 10^{-23} \text{ kg m}^{-3}$, one has

$$\frac{1}{t_{\text{df}}} \simeq 1.225 \times 10^{-17} \text{ s}^{-1}, \quad \gamma = \frac{1}{\tau_{\text{ch}}} = \frac{t_0}{t_{\text{df}}} \simeq 0.0032. \quad (76)$$

We intend to insert these values into the hydrodynamic framework of DM evolution, assuming they remain constant as the star cluster shifts from $\check{r} = 1.1 \text{ kpc}$ by $0.1r_0$. The dynamics of the cluster itself are omitted here.

3.4 Hydrodynamic DM evolution induced by three processes

Since the mass of a single baryonic cluster is an order of magnitude smaller than the total baryonic mass of the galaxy, which itself is roughly an order of magnitude smaller than the DM mass, no significant changes in the DM density profile are expected across the three scenarios proposed above. To study these effects in detail, we need linearized equations describing the hydrodynamic evolution of DM perturbations induced by baryonic processes.

Therefore, for a relatively small magnitude of the velocity $v(\xi, \tau) = \delta v(\xi, \tau)$, the quadratic term v^2 in (28) can be omitted. The variation of the DM density, $\delta\eta(\xi, \tau)$, relative to the stationary distribution $\eta(\xi)$ that satisfies (25), produces the following modifications in the interaction term and quantum pressure:

$$W[\sqrt{\eta + \delta\eta}] = W[\sqrt{\eta}] + A\Delta_\xi^{-1}\delta\eta + c_s^2 \frac{\delta\eta}{\eta} + O(\delta\eta^2), \quad (77)$$

$$\frac{\Delta_\xi \sqrt{\eta + \delta\eta}}{\sqrt{\eta + \delta\eta}} = \frac{\Delta_\xi \sqrt{\eta}}{\sqrt{\eta}} + \frac{1}{2} \left[\Delta_\xi + \frac{\partial_\xi \eta}{\eta} \partial_\xi \right] \frac{\delta\eta}{\eta} + O(\delta\eta^2), \quad (78)$$

where the square of the sound speed c_s^2 and the self-gravity potential variation are

$$c_s^2 \equiv \eta \frac{dj_0(\sqrt{\eta})}{d\eta} = -\frac{\sqrt{\eta}}{2} j_1(\sqrt{\eta}), \quad (79)$$

$$\Delta_\xi^{-1} \delta\eta(\xi, \tau) = \int_0^\xi \left(\frac{1}{s} - \frac{1}{\xi} \right) \delta\eta(s, \tau) s^2 ds + C(\tau). \quad (80)$$

The integral

$$C(\tau) = - \int_0^{\xi_B} \delta\eta(s, \tau) s ds \quad (81)$$

is irrelevant in the hydrodynamic equations, but it does contribute to the phase θ .

Since the DM density $\eta(\xi)$ is a solution to (25), one has that

$$-\frac{\Delta_\xi \sqrt{\eta}}{\sqrt{\eta}} + W[\sqrt{\eta}] = 2u, \quad (82)$$

where u is the constant chemical potential.

Given (47) and (50), necessary to account for the redistribution of baryons, we need to subtract the gravitational potential of the initial configuration from the chemical potential, and then add the potential of the new configuration. To an infinitesimal approximation, this yields the following replacement:

$$2u \rightarrow 2u + \delta\Phi_b(\xi, \tau), \quad (83)$$

writing the time-dependent potential difference as

$$\delta\Phi_b(\xi, \tau) = \Phi_\ell(\xi, \check{\xi}, \ell) \delta\ell(\tau) + \Phi_\xi(\xi, \check{\xi}, \ell) \delta\check{\xi}(\tau). \quad (84)$$

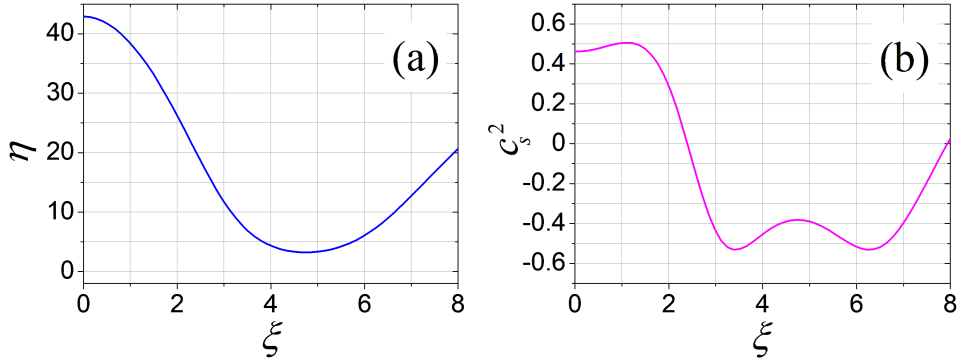


Figure 4: Equilibrium DM density η and the squared speed of sound c_s^2 .

We assume that the underlying equilibrium density $\eta(\xi)$ remains unchanged in all our scenarios. Moreover, we impose the same initial conditions:

$$\delta\eta(\xi, 0) = 0, \quad v(\xi, 0) = 0. \quad (85)$$

Thus, the set of hydrodynamic equations reads

$$\partial_\tau \delta\eta(\xi, \tau) + \frac{1}{\xi^2} \partial_\xi [\xi^2 \eta(\xi) v(\xi, \tau)] = 0, \quad (86a)$$

$$2\partial_\tau v(\xi, \tau) + \partial_\xi \mathbb{V}(\xi, \tau) = 0, \quad (86b)$$

where we have introduced auxiliary potential:

$$\mathbb{V}(\xi, \tau) = A_b \delta\Phi_b(\xi, \tau) + A \Delta_\xi^{-1} \delta\eta(\xi, \tau) + \left[c_s^2(\xi) - \frac{\Delta_\xi}{2} - \frac{\partial_\xi \eta(\xi)}{2\eta(\xi)} \partial_\xi \right] \frac{\delta\eta(\xi, \tau)}{\eta(\xi)}. \quad (87)$$

Furthermore, we impose the boundary conditions:

$$\delta\eta'(0, \tau) = 0, \quad v(0, \tau) = 0, \quad (88a)$$

$$\delta\eta(\xi_B, \tau) = 0, \quad v(\xi_B, \tau) = 0. \quad (88b)$$

The prime at $\delta\eta$ denotes the derivative with respect to ξ .

Conditions (88a) exclude divergences at $\xi = 0$ in spherical symmetry. The two conditions in (88b) ensure the DM halo radius ξ_B remains unchanged, preventing changes in the chemical potential or hydraulic pressure if the kinetic term $\sim v^2$ is added.

To apply the equations to the DM in NGC 2366, we set $A = 0.0045$ and $\xi_B = 6.65$, and employ the numerically obtained $\eta(\xi)$ and $c_s^2(\xi)$ shown in figure 4.

3.4.1 Gas cluster expansion

Consider the hypothetical expansion of gas cluster-1 as it widens from the width $d_{\text{in}} = 0.09$ kpc to the observed $d_{\text{fin}} = 0.23$ kpc with a fixed center $\check{r} = 1.1$ kpc, likely due to a starburst or explosion. We associate the initial geometry with star cluster-2 in table 2 and adopt the final configuration of gas cluster-1 in table 1. We also admit the conservation of gas mass in this process.

In general, photoionization, supernovae, and stellar winds act as stellar feedback, heating surrounding gas and dispersing dense clouds, thereby suppressing further star formation. Feedback from existing stars typically reduces the efficiency of new star formation. Yet feedback can also be positive – shock-driven turbulence may compress cool gas, causing the collapse of dense regions and stimulating star formation.

Carrying out the modeling in dimensionless quantities, we rewrite the initial and final parameters of the gas cluster in units of $r_0 = 1.18$ kpc:

$$\check{\xi} = 0.932, \quad \ell_{\text{in}} = 0.076, \quad \ell_{\text{fin}} = 0.195, \quad \delta\ell_\infty = 0.119. \quad (89)$$

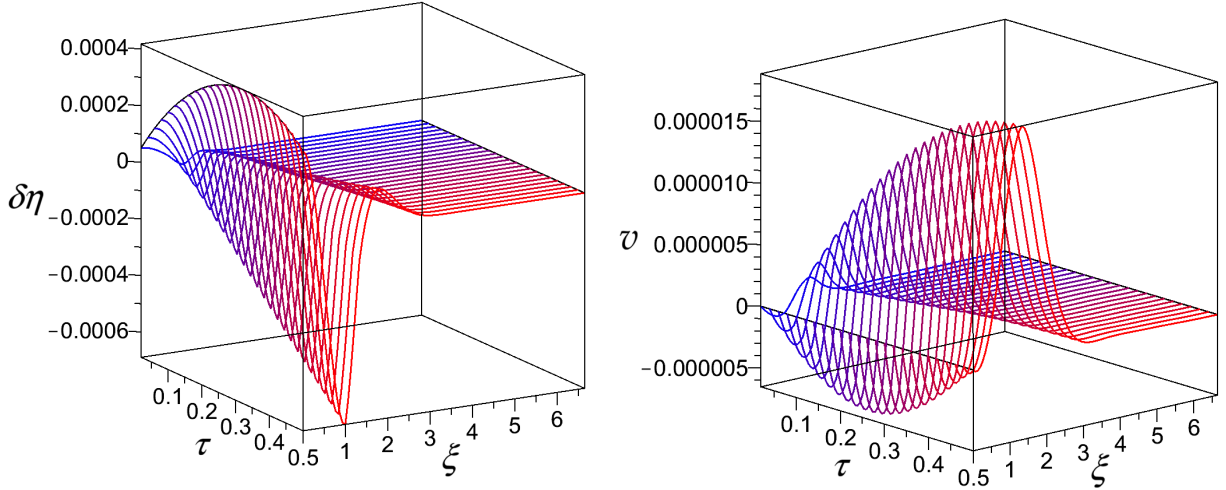


Figure 5: DM perturbation density $\delta\eta$ and velocity v during the expansion of gas cluster-1.

Having obtained $A_b = 0.0031$ by substituting the mass of gas cluster-1 into (46), we model the change in the baryon gravitational potential over time as

$$\begin{aligned} \Delta\Phi_b(\xi, \tau) &= \Phi_b(\xi, \check{\xi}, l_{\text{fin}} - \delta l_\infty e^{-\gamma\tau}) - \Phi_b(\xi, \check{\xi}, l_{\text{fin}} - \delta l_\infty) \\ &\simeq \Phi_\ell(\xi, \check{\xi}, l_{\text{fin}}) \delta l_\infty (1 - e^{-\gamma\tau}), \end{aligned} \quad (90)$$

$$\Delta\Phi_b(\xi, 0) = 0, \quad (91)$$

where Φ_ℓ appears in (53), and γ is associated with the inverse characteristic time $1/\tau_{ch}$.

By equating τ_{ch} to the time of gravitational impact of the expanding gas on the DM, one can roughly estimate the average velocity of the gas:

$$v_{\text{gas}} \sim v_0 \frac{\delta l_\infty}{\tau_{ch}} = v_0 \gamma \delta l_\infty \simeq 16.5 \gamma \text{ km/s}, \quad (92)$$

where v_0 is taken from (40).

Velocity observations indicate that the cases $\gamma \sim 5 - 50$ are the most likely. We set

$$\tau_{ch} = 0.1, \quad \gamma = 10. \quad (93)$$

For comparison, the gas escape velocity can be estimated from the combined gravitational potentials of gas cluster-1 (“gc1”) and star cluster-2 (“sc2”) as infinitely thin shells. By Gauss’s theorem, such potentials coincide with the corresponding spherical potentials to give

$$v_{\text{esc}} = \sqrt{2G \frac{M_{\text{gc1}} + M_{\text{sc2}}}{\check{r}}} \simeq 13.84 \text{ km/s}, \quad (94)$$

where $\check{r} = \check{r}_{\text{gc1}} = \check{r}_{\text{sc2}} = 1.1 \text{ kpc}$ specifies the joint position of the clusters whose masses $M_{\text{gc1}} \simeq 8.042 \times 10^6 M_\odot$ and $M_{\text{sc2}} \simeq 16.34 \times 10^6 M_\odot$ are taken from table 1 and 2.

Since the gas expansion occurs rapidly over the time interval $0 \leq \tau \leq \tau_{ch}$, the hydrodynamics of the accompanying DM perturbations is governed primarily by the force arising from the gravitational potential $\delta\Phi_b$. Quantum fluctuations do not develop at this stage, and the velocity profile v evolves predominantly in accordance with the scaling law. Therefore, figure 5 shows the density $\delta\eta$ and velocity v profiles already for $\tau = \tau_{ch}$. The velocity profile describes the DM winds in opposite directions from the cluster center, near $\xi = 0.932$, where $\delta\eta < 0$. However, this wave-like motion leads to $\delta\eta > 0$ in regions located farther from the explosion site.

Even after the baryon distribution has stabilized, DM disturbances continue to evolve. Although the analysis for times $\tau > \tau_{ch}$ in principle requires a model adjustments, we estimate the

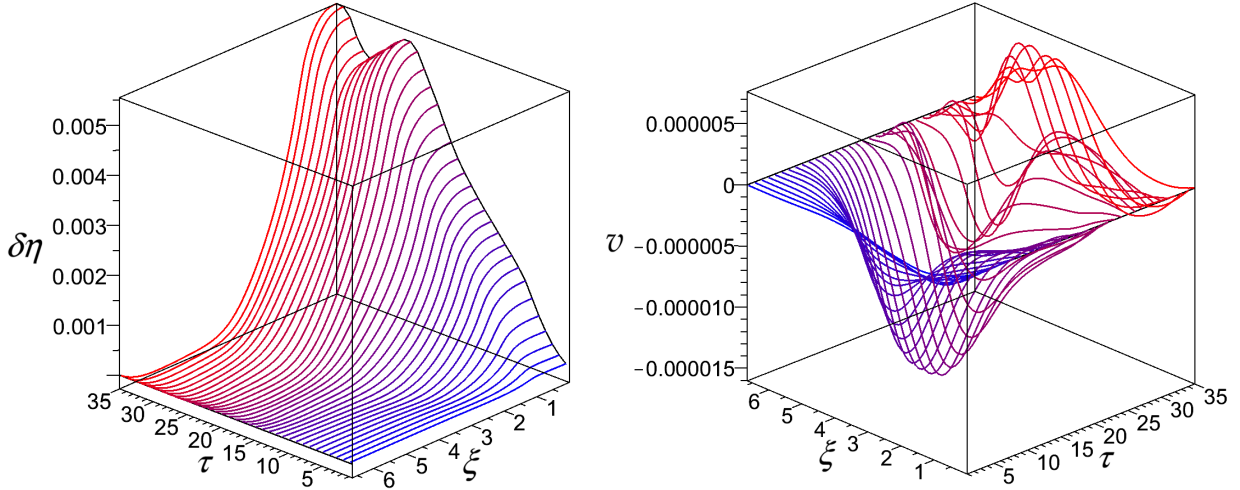


Figure 6: DM perturbation density $\delta\eta$ and velocity v during the collapse of gas cluster-1.

scale of subsequent perturbations as before, up to $\tau = 5\tau_{ch}$ in figure 5. During this time, the velocity directed toward the halo center reverses direction, resembling a reflection. Simultaneously, figure 5(left) shows an outflow of DM particles from the halo center.

It is crucial that both the velocity v (a few meters per second) and the density deviation $\delta\eta$ (giving $\delta\eta/\eta \sim 10^{-5}$) remain small for a long time. This stability is maintained even when disturbances arise in the region $\xi \in [2.41; 6.65]$, corresponding to the DM unstable phase, characterized by $c_s^2 < 0$ in figure 4b. This can be attributed to the fact that quantum fluctuations develop after the end of the gas expansion that initiated the disturbance and had a speed exceeding the DM speed of sound c_s at $\xi < 2.4$. Despite the low velocity v of the DM winds, the wave-peak widths reach kiloparsec scales. This may be due to the contribution of long-wavelength quantum fluctuations.

Note that obtaining accurate numerical solutions for high-order inhomogeneous equations on large time scales is challenging. However, using both a centered implicit scheme with adaptive steps and time scale variation, $\tau' = \zeta\tau$, provides reliable results and robust conclusions for all scenarios. Furthermore, we refrained from deriving closed equations of even higher order to avoid the influence of homogeneous solutions due to complex kernels.

3.4.2 Gas cluster collapse

Let us analyze the implications of the process inverse to that considered above – the collapse (narrowing) of gas cluster-1, which facilitates star formation.

The gravitational effect of the gas mass concentration can be described using the potential at $A_b = 0.0031$:

$$\begin{aligned} \Delta\Phi_b(\xi, \tau) &= \Phi_b(\xi, \check{\xi}, l_{\text{fin}} - \delta l_\infty e^{-\gamma\tau}) - \Phi_b(\xi, \check{\xi}, l_{\text{in}}) \\ &\simeq -\Phi_\ell(\xi, \check{\xi}, l_{\text{in}}) |\delta l_\infty| (1 - e^{-\gamma\tau}), \end{aligned} \quad (95)$$

for $\delta l_\infty = -|\delta l_\infty|$, and

$$\check{\xi} = 0.932, \quad l_{\text{fin}} = 0.076, \quad l_{\text{in}} = 0.195, \quad |\delta l_\infty| = 0.119. \quad (96)$$

This means that the average density of the gas mass increases from $\bar{\rho}_{\text{gc}} \simeq 5.5 \times 10^{-23} \text{ kg m}^{-3}$ to $1.42 \times 10^{-22} \text{ kg m}^{-3}$ according to (35). Although the final value does not yet reach the star formation threshold in density [73], we are only interested in the gravitational perturbation created by the compaction. Stars that are accreting mass from the surrounding gas cloud are considered protostars.

To estimate the timescale of gas concentration within star cluster-2 using the free-fall time of gas, we invoke the conservation of energy expressed in dimensionless form:

$$\left(\frac{d\xi}{d\tau}\right)^2 = A_b \left[\Phi(\xi, \check{\xi}, \ell_{\text{in}}) - \Phi(\xi, \check{\xi}, \ell_{\text{fin}}) \right], \quad (97)$$

where the average initial velocity of the gas is assumed to be zero, and the gravitational background created by star cluster-2 remains unchanged. Then we set

$$\tau_{ch} = \max(\tau_{\rightarrow}, \tau_{\leftarrow}), \quad (98)$$

where τ_{\rightarrow} and τ_{\leftarrow} are the moments of approaching the shell core from opposite sides:

$$\tau_{\rightarrow} = \int_{\check{\xi}-\ell_{\text{in}}}^{\check{\xi}} \frac{d\xi}{\sqrt{A_b \Phi_{\ell}(\xi, \check{\xi}, \ell_{\text{in}}) |\delta\ell_{\infty}|}} \simeq 14.46, \quad (99a)$$

$$\tau_{\leftarrow} = - \int_{\check{\xi}+\ell_{\text{in}}}^{\check{\xi}} \frac{d\xi}{\sqrt{A_b \Phi_{\ell}(\xi, \check{\xi}, \ell_{\text{in}}) |\delta\ell_{\infty}|}} \simeq 16.00. \quad (99b)$$

Thus, we choose

$$\tau_{ch} = 16, \quad \gamma = 0.0625. \quad (100)$$

The mean velocity of the self-gravitating gas,

$$v_{\text{gas}} = \frac{|\delta\ell_{\infty}|}{\tau_{ch}} v_0 \simeq 1.03 \text{ km/s}, \quad (101)$$

exceeds the sound speed of a cold molecular gas. This indicates that gravitational forces may accidentally outweigh the supporting pressure, leading to gas instability and its collapse according to the Jeans criteria.

When compared, the potentials $\delta\Phi_b(\xi, \tau)$ that drive the expansion and collapse of the same gas cluster-1 have opposite signs and characteristic times that differ by two orders of magnitude. This disparity implies that substantial quantum fluctuations should develop upon reaching the moment $\tau = \tau_{ch}$ in the event of collapse. These fluctuations, in turn, affect the formation of the perturbed density $\delta\eta$ and velocity v profiles shown in figure 6, obtained by using the time variable $\tau' = 0.1\tau$ when integrating the hydrodynamic equations.

By considering the time interval up to $\tau \simeq 2\tau_{ch}$ in figure 6, two clear trends emerge. During the slow gas collapse the induced dark-wind velocity v is roughly an order of magnitude smaller than during the rapid gas expansion. By contrast, the perturbed density $\delta\eta$ turns out about an order of magnitude larger in the collapse than in the expansion, by comparing figure 5 and 6.

Thus, for $\tau \leq 35$ ($t \leq 291$ Myr), the DM configuration remains effectively unchanged in response to the gas cluster collapse, although additional events should be expected on these timescales. Nevertheless, it can be assumed that slow baryon flows induce a noticeable alteration of the DM density.

3.4.3 Star cluster migration

To confirm the dominant role of slow baryonic mechanisms in DM redistribution and to complete the picture of how stellar displacements affect DM, we model the migration of the entire star cluster-2 towards the galactic center, driven by dynamical friction in the surrounding gas cluster-1.

Under the assumption of constant cluster mass during its migration to the hypothetical radius $\check{r}_{\text{fin}} = 0.832r_0$, the process is characterized by the following dimensionless geometric parameters:

$$\check{\xi}_{\text{in}} = 0.932, \quad \ell_{\text{in}} = 0.076, \quad \check{\xi}_{\text{fin}} = 0.832, \quad \delta\check{\xi}_{\infty} = 0.1, \quad (102)$$

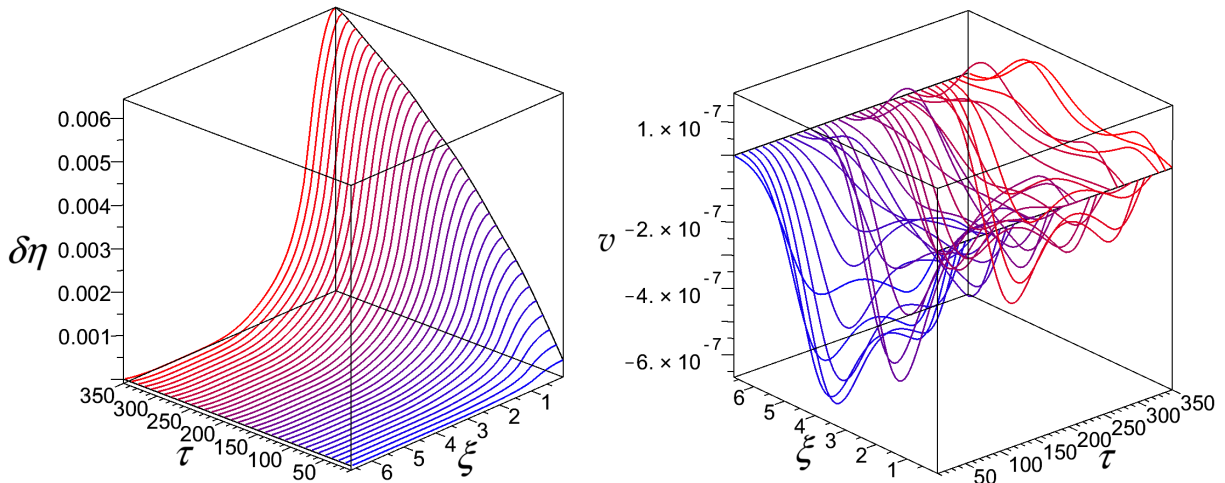


Figure 7: DM perturbation density $\delta\eta$ and velocity v during the migration of star cluster-2.

along with the dynamical ones

$$\tau_{ch} = 312.5, \quad \gamma = 0.0032. \quad (103)$$

To estimate a conservative upper bound $\gamma = t_0/t_{df}$ for the inward migration rate in the gas cluster-1 environment with the mean mass density $\bar{\rho}_{gc} \simeq 5.5 \times 10^{-23} \text{ kg m}^{-3}$, we use dynamical-friction scaling (75) for the mass $M_{sc} = 16.34 \times 10^6 M_\odot$ and the position $\tilde{r} = 1.1 \text{ kpc}$ of both clusters from table 1 and 2. The rotation velocity of the stars $V_t = 22 \text{ km/s}$, taken from the rotation curve of NGC 2366 in [28, 59], significantly exceeds the sound speed in cold gas.

Computing the gravitational parameter $A_b = 0.00622$, we modify the potential as

$$\begin{aligned} \Delta\Phi_b(\xi, \tau) &= \Phi_b(\xi, \check{\xi}_{fin} + \delta\check{\xi}_\infty e^{-\gamma\tau}, l_{in}) - \Phi_b(\xi, \check{\xi}_{in}, l_{in}) \\ &\simeq -\Phi_\xi(\xi, \check{\xi}_{in}, l_{in}) \delta\check{\xi}_\infty (1 - e^{-\gamma\tau}). \end{aligned} \quad (104)$$

The hydrodynamic evolution of DM induced by the slow migration of star cluster-2, over timescales much longer than in previous gas-based scenarios, is shown in figure 7 and is the result of integrating the equations with auxiliary time variable $\tau' = 0.01\tau$. This confirms the correlation between a low rate and a large perturbation in DM density. Furthermore, by tracking the longest process, we observe the decay of the DM wind through a comparison of velocity magnitudes at the beginning and end of the time interval in figure 7. Despite its low velocity of the order of 1 cm/s, the widths of its wave peaks are enormous. We again observe an increase in wind speed in the region of the unstable phase of DM at $\xi > 2.4$.

Based on the three scenarios considered, we reach a preliminary conclusion: if the motions of gas and star clusters induce only minor perturbations in DM, then even small excitations of DM may exert a significant gravitational impact on galactic baryonic matter. This effect is most likely when large fluctuations in DM density or velocity occur on short spatial scales over sufficient time intervals.

At present, the specific mechanisms capable of producing such fluctuations remain uncertain. Nevertheless, a plausible pathway is a shock transition of the DM wind from an unstable phase region, in which a pronounced increase in velocities is typically observed, to a stable one with a finite speed of sound.

4 Multiple events and decay of excitations

To assess the influence of spatially and temporally separated subgalactic baryonic processes on DM, we proceed as follows. Since the relaxation of each process cannot be disentangled from the

background of others, we treat their effects as small perturbations, thereby excluding resonance phenomena and assuming conservation of the total DM content. The gravitational potentials generated by these processes are then summed in the infinite-time limit. Moreover, they may be further averaged as in (48) and incorporated into the constant chemical potential to compute the final (quasi-)stationary distribution of DM. The thermodynamic functions of DM in the galaxy NGC 2366, derived from its distributions for varying values of the chemical potential, are already presented in [28].

However, this approach is valid under the condition of hydrodynamic relaxation of DM flows. It means, at minimum, the relaxation of initial perturbations in the original configuration – namely, the solutions of the homogeneous hydrodynamic equations. In the absence of viscosity, damping can only be provided by quantum effects in the presence of instability. Therefore, in what follows, we focus on attenuation of a quantum nature.

Since the phase θ of the macroscopic wave function is the potential for the collective velocity, $v = \partial_\xi \theta$, the linearized homogeneous equation for it is

$$2\partial_\tau^2 \theta(\xi, \tau) - c_s^2(\xi) \tilde{\Delta}_\xi \theta(\xi, \tau) + \frac{\tilde{\Delta}_\xi^2}{2} \theta(\xi, \tau) - A \Delta_\xi^{-1} \left[\eta(\xi) \tilde{\Delta}_\xi \theta(\xi, \tau) \right] = 0, \quad (105)$$

$$\tilde{\Delta}_\xi \equiv \frac{1}{\xi^2 \eta(\xi)} \partial_\xi \xi^2 \eta(\xi) \partial_\xi = \Delta_\xi + \frac{\partial_\xi \eta(\xi)}{\eta(\xi)} \partial_\xi, \quad (106)$$

where, as before, we impose the boundaries $v(0, \tau) = v(\xi_B, \tau) = 0$. For the steady state model with the particle density $\eta(\xi)$ and square of sound speed $c_s^2(\xi)$, $\theta = -u\tau$ serves as a solution of (105) at constant chemical potential u in dimensionless units.

For uniform spherically symmetric system with constant density $\eta = \text{const}$ and sound speed c_s , the modified Laplace operator $\tilde{\Delta}_\xi$, representing the divergence of the gradient in hydrodynamics, coincides with the ordinary one, $\tilde{\Delta}_\xi = \Delta_\xi$. The solution to (105) is then obtained by separating the variables for each n -th mode $\cos(\omega_n \tau) f_n(\xi)$ in the finite interval $\xi \in [0; \xi_B]$, which is given by the orthonormal spherical waves

$$f_0(\xi) = \sqrt{\frac{3}{\xi_B^3}}, \quad f_{n>0}(\xi) = \sqrt{\frac{2}{\xi_B^3}} \frac{j_0(k_n \xi)}{j_0(k_n \xi_B)}, \quad k_n = \frac{a_n}{\xi_B}, \quad (107)$$

where a_n is the n -th zero of function $j_0'(a_n) = -j_1(a_n) = 0$.

Taking into account that $\Delta_\xi f_n(\xi) = -k_n^2 f_n(\xi)$, the dispersion relation reproduces the Bogolyubov spectrum of quasiparticles in dimensionless variables:

$$\omega_n = \pm \sqrt{\frac{k_n^4}{4} + \frac{1}{2}(c_s^2 k_n^2 - A\eta)}. \quad (108)$$

The excitation energy ω_n is real when $k_n > k_{\text{th}}$ for some threshold wave number k_{th} [34, 35]. However, at $k_n < k_{\text{th}}$ the spectrum becomes imaginary, indicating either unstable or metastable states, what we have to find out in detail and apply.

In general, we need to find the eigenvectors and eigenvalues of the operator

$$\hat{L} = \frac{1}{2} \tilde{\Delta}_\xi^2 - c_s^2(\xi) \tilde{\Delta}_\xi - A \Delta_\xi^{-1} \eta(\xi) \tilde{\Delta}_\xi. \quad (109)$$

It is appropriate to start by studying the spectrum of the hydrodynamic Laplace operator $\tilde{\Delta}_\xi$, taking into account that

$$\tilde{\Delta}_\xi \frac{\varphi(\xi)}{\sqrt{\eta(\xi)}} = \frac{1}{\sqrt{\eta(\xi)}} [\Delta_\xi - V_L(\xi)] \varphi(\xi), \quad V_L(\xi) \equiv \frac{1}{\sqrt{\eta(\xi)}} \Delta_\xi \sqrt{\eta(\xi)}, \quad (110)$$

where the potential V_L , which coincides with the quantum pressure term, is shown in figure 8. The potential possesses a well of finite depth within $\xi \in [0; 2.75]$, bounded on the right by

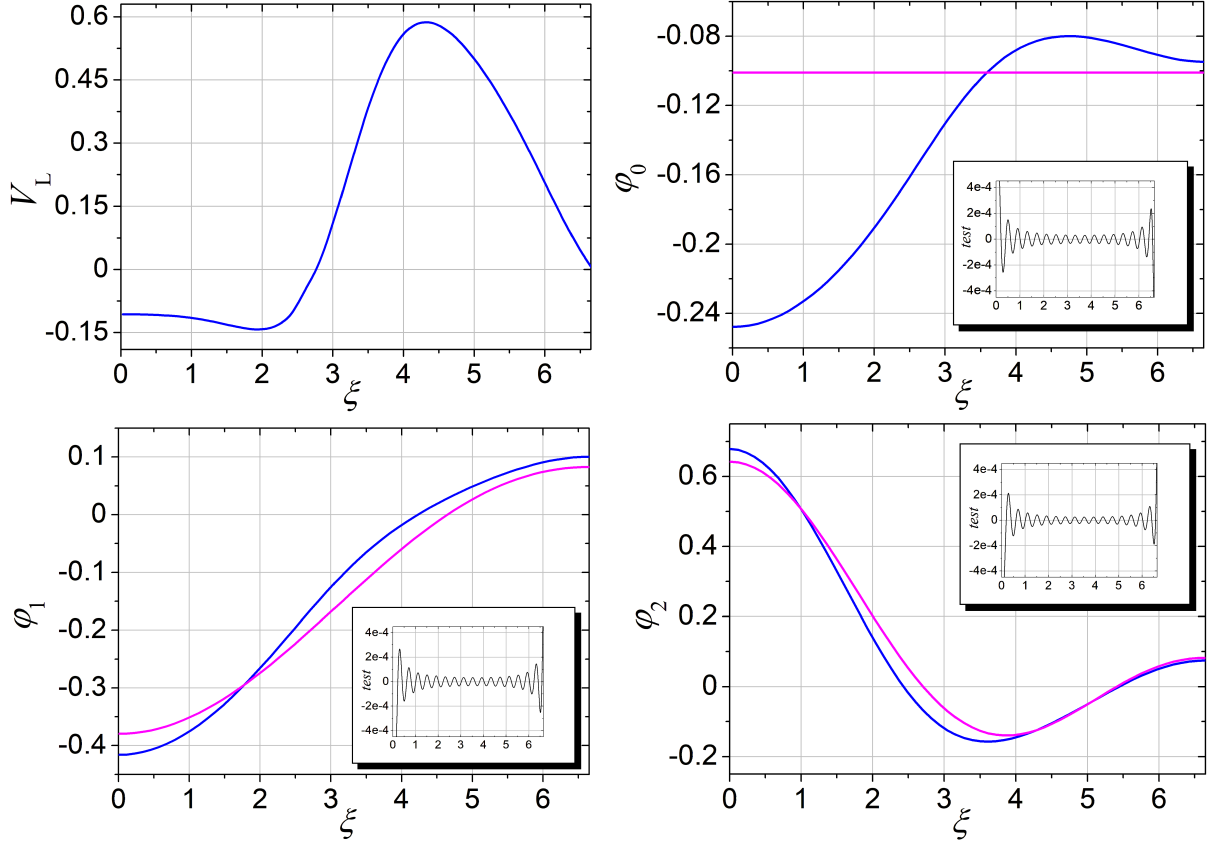


Figure 8: Potential V_L and wave functions φ_n (blue), compared with wave functions f_n (magenta). The index n denotes the number of nodes within the interval $\xi \in [0; \xi_B]$; $\xi_B = 6.65$. Nested plots labeled “test” show the local values of $[\Delta_\xi - V_L - \lambda_n]\varphi_n$.

a barrier of finite height. Such a configuration supports metastable states, which may decay through quantum tunneling across the barrier. Besides, this feature is confirmed by other potentials in this particular case, shown in Fig. 7 in [28].

Thus, we are faced with the auxiliary problem:

$$[\Delta_\xi - V_L(\xi)] \varphi_n(\xi) = \lambda_n \varphi_n(\xi), \quad (111)$$

by imposing the boundaries $\varphi'_n(0) = 0$ and $\varphi'_n(\xi_B) = 0$.

The equation (111) with $\lambda_n < 0$ is equivalent to the stationary Schrödinger equation with positive energy. In this regime, a particle subject to the finite potential V_L , confined within the spatial interval $\xi \in [0; \xi_B]$, should experience its influence less and less as the energy $-\lambda_n$ increases.

We expand the functions $\{\varphi_n\}$ in the orthonormal basis $\{f_n\}$ from (107):

$$\varphi_m(\xi) = \sum_{n=0}^{n_{\max}} A_{m,n} f_n(\xi), \quad n_{\max} \rightarrow \infty. \quad (112)$$

Technically, when defining the first few states, we limit ourselves to the value $n_{\max} = 32$.

By numerically calculating the eigenvectors and values of the symmetric matrix

$$D_{n,m} = \int_0^{\xi_B} f_n(\xi) [\Delta_\xi - V_L(\xi)] f_m(\xi) \xi^2 d\xi = -k_n^2 \delta_{n,m} - (V_L)_{n,m}, \quad (113)$$

we compare the orthonormal wave functions φ_n and f_n in figure 8 and the “energies” in table 3.

n	$\lambda_n = -\kappa_n^2$	$-k_n^2$	$-k_n^2 - (V_L)_{n,n}$
0	-0.25485939	0	-0.29424677
1	-0.49297465	-0.45657139	-0.50596328
2	-1.54638409	-1.34952831	-1.52447396
3	-2.84678233	-2.68867364	-2.83908790
4	-4.63735537	-4.47414351	-4.63244151
5	-6.86658836	-6.70596223	-6.86374358
6	-9.54439985	-9.38413675	-9.54231141
7	-12.6685089	-12.5086697	-12.6669947
8	-16.2391606	-16.0795624	-16.2379838
9	-20.2562436	-20.0968154	-20.2553091
10	-24.7197351	-24.5604291	-24.7189730

Table 3: The first eigenvalues of the Laplace operators $\tilde{\Delta}_\xi$ and Δ_ξ . The last column shows the eigenvalues in the mean field approximation (MFA).

Significant discrepancies between φ_n and f_n are evident for small n . However, as n increases, the two wave functions become nearly indistinguishable for $n \geq 5$. The relative difference between $\lambda_n = -\kappa_n^2$ and $-k_n^2 - (V_L)_{n,n}$ in the mean field approximation (MFA) tends to zero.

By construction, orthogonality of the set $\{\varphi_n\}$ is exact:

$$\delta_{n,m} = \int_0^{\xi_B} \varphi_n(\xi) \varphi_m(\xi) \xi^2 d\xi. \quad (114)$$

The pseudo-Hermitian operator (109) acts on the chosen basis as

$$\sqrt{\eta} \hat{L} \frac{\varphi_n}{\sqrt{\eta}} = \frac{\lambda_n^2}{2} \varphi_n - \lambda_n c_s^2 \varphi_n - A \lambda_n \sqrt{\eta} \Delta_\xi^{-1} (\sqrt{\eta} \varphi_n). \quad (115)$$

Therefore, the expression for the matrix element of \hat{L} in the basis $\{\varphi_n\}$ becomes

$$\begin{aligned} (\hat{L})_{m,n} &\equiv \int_0^{\xi_B} d\xi \xi^2 \eta \left(\frac{\varphi_m}{\sqrt{\eta}} \right) \hat{L} \left(\frac{\varphi_n}{\sqrt{\eta}} \right) \\ &= \frac{\lambda_n^2}{2} \delta_{m,n} - \lambda_n \int_0^{\xi_B} d\xi \xi^2 \left[\varphi_m c_s^2 \varphi_n + A (\varphi_m \sqrt{\eta}) \Delta_\xi^{-1} (\sqrt{\eta} \varphi_n) \right]. \end{aligned} \quad (116)$$

The spectrum $\{\Lambda_n\}$ of \hat{L} is then defined from the equation $\det \|(\hat{L})_{m,n} - \Lambda \delta_{m,n}\| = 0$.

Using auxiliary Hermitian matrices

$$\hat{Q} = \left\| \frac{\delta_{n,m}}{\sqrt{-\lambda_n}} \right\|, \quad \hat{Q}^{-1} = \left\| \sqrt{-\lambda_n} \delta_{n,m} \right\|, \quad (117)$$

the pseudo-Hermitian matrix \hat{L} is transformed into a Hermitian one:

$$\hat{L}_Q = \hat{Q}^{-1} \hat{L} \hat{Q}. \quad (118)$$

This saves the spectrum in table 4, but the eigenvectors $\vec{u}_n = (B_{m,n})$ of the symmetric matrix \hat{L}_Q provide the orthogonality of the normalized wave functions:

$$\psi_m(\xi) = \sum_{n=0}^{n_{\max}} B_{m,n} \varphi_n(\xi), \quad m = 0, 1, \dots, n_{\max}, \quad (119)$$

some of them are shown in figure 9. This is due to the following properties:

$$\sum_{n=0}^{n_{\max}} B_{n,m} B_{n,k} \equiv \vec{u}_m^\top \vec{u}_k = \delta_{m,k}, \quad \sum_{n=0}^{n_{\max}} B_{m,n} B_{k,n} = \delta_{m,k}. \quad (120)$$

n	$\Lambda_n = 2\omega_n^2$	$(\widehat{L})_{n,n}$
0	-0.21917569	-0.20713777
1	-0.06773034	-0.01407956
2	0.85494467	0.88022226
3	3.51951730	3.57976534
4	10.0160435	10.0622828
5	22.5504876	22.5988944
6	44.1887648	44.2362758
7	78.4924233	78.5390662
8	129.651974	129.698339
9	202.447854	202.493856
10	302.259683	302.305455

Table 4: The first eigenvalues of \widehat{L} . The last column shows the MFA values.

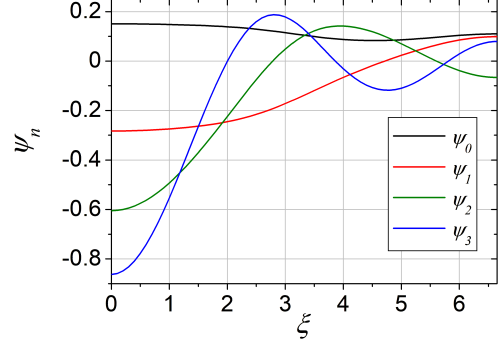


Figure 9: Eigenfunctions of \widehat{L}_Q over the interval $\xi \in [0; 6.65]$.

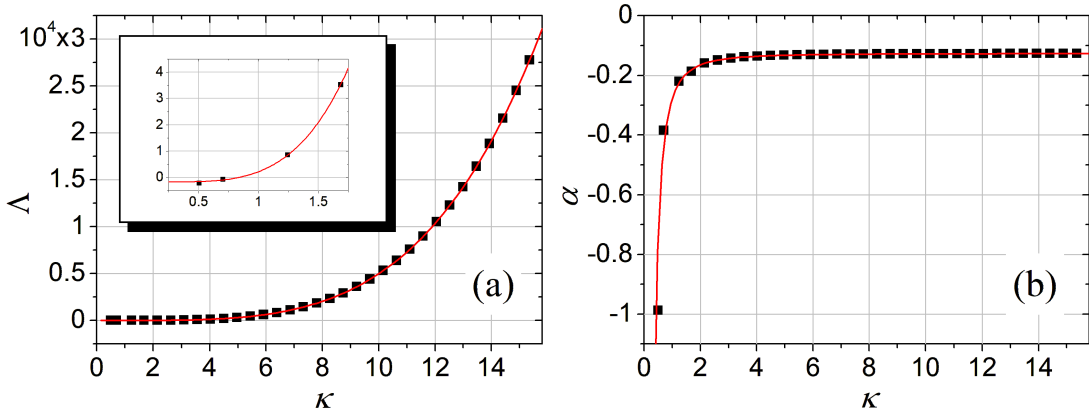


Figure 10: Spectrum of the operator \widehat{L} (a) and the function α (b) from relation (122). Black squares represent the values of Λ_n . Red lines are plotted using the fit (123).

The set of non-orthogonal eigenfunctions $\widetilde{\psi}_n$ of the operator \widehat{L} is then calculated as

$$\widetilde{\psi}_m(\xi) = \sum_{n=0}^{n_{\max}} \frac{B_{m,n}}{\sqrt{-\lambda_n}} \varphi_n(\xi). \quad (121)$$

The central issue at this stage is whether the spectrum can be expressed in the form:

$$\Lambda(\kappa) = \frac{\kappa^4}{2} + \alpha(\kappa)\kappa^2, \quad \Lambda_n = \Lambda(\kappa_n), \quad (122)$$

where $\alpha(\kappa)$ takes into account the contribution of the non-uniform speed of sound and gravity for the wave number $\kappa = \sqrt{-\lambda}$ in the medium.

The unstable phase, characterized by $c_s^2(\xi) < 0$, together with the self-gravity of DM, leads to negative values of $\alpha \in [-0.9874; -0.1269]$ in the given range of κ . Moreover, the eigenvalues Λ_0 and Λ_1 in table 4 are negative, and the associated oscillation modes have $\omega_{0,1}^2 < 0$. This reflects the Jeans instability in the long-wave range.

Given that gravity makes a contribution $\sim \kappa^{-2}$, the best fit to $\alpha(\kappa)$ is

$$\alpha_{\text{fit}}(\kappa) = -0.12627 - \frac{0.153}{\kappa^2}. \quad (123)$$

Examining the dependence $\Lambda(\kappa)$ in figure 10a, we see that the modes become stable at $\kappa \geq 1$, when $\Lambda(\kappa) > 0$. As κ increases, $\alpha(\kappa)$ rapidly approaches its maximal value $\alpha_{\max} \simeq -0.1269$,

as shown in figure 10b. Substituting (123) into (122), we obtain approximate spectrum $\Lambda(\kappa)$, which differs slightly from the exact result at $\kappa < 1$.

Combining, a solution to (105) can be written in the form [74]:

$$\theta(\xi, \tau) = \sum_{n,m} B_{n,m} \left(\frac{|\omega_n|}{2\eta(\xi)\kappa_m^2} \right)^{1/2} (\beta_n e^{-i\omega_n\tau} + \bar{\beta}_n e^{i\omega_n\tau}) \varphi_m(\xi), \quad (124)$$

where we substituted (121); β_n and $\bar{\beta}_n$ are complex conjugate amplitudes, which are defined by initial conditions; and the cyclic frequency

$$\omega_n = \omega(\kappa_n), \quad \omega(\kappa) = \sqrt{\frac{\kappa^4}{4} + \alpha(\kappa)\frac{\kappa^2}{2}}. \quad (125)$$

Due to the continuity relation $\partial_\tau \delta\eta = -\eta \tilde{\Delta}_\xi \theta$, we derive the density perturbation:

$$\delta\eta(\xi, \tau) = i \sum_{n,m} B_{n,m} \left(\frac{\eta(\xi)\kappa_m^2}{2|\omega_n|} \right)^{1/2} (\beta_n e^{-i\omega_n\tau} - \bar{\beta}_n e^{i\omega_n\tau}) \varphi_m(\xi). \quad (126)$$

Furthermore, we promote the amplitudes to bosonic creation and annihilation operators, $\bar{\beta}_n \rightarrow \hat{\beta}_n^\dagger$ and $\beta_n \rightarrow \hat{\beta}_n$, which satisfy the canonical commutation relation:

$$[\hat{\beta}_n, \hat{\beta}_m^\dagger] \equiv \hat{\beta}_n \hat{\beta}_m^\dagger - \hat{\beta}_m^\dagger \hat{\beta}_n = \delta_{n,m}. \quad (127)$$

Using (120), the commutator of quantized fields at the same τ is reduced to

$$\left[\widehat{\theta}(\xi_1, \tau), \widehat{\delta\eta}(\xi_2, \tau) \right] = -i \sum_n \varphi_n(\xi_1) \varphi_n(\xi_2) = -\frac{i}{\xi_1 \xi_2} \delta(\xi_1 - \xi_2), \quad (128)$$

where the last equality is valid for the complete set $\{\varphi_n\}$, when $n_{\max} \rightarrow \infty$.

The form of fields (124) and (126), as well as their versions with quantized amplitudes, could also be obtained using the Bogolyubov transform, taking into account the presence of unstable modes as in [75–77].

The starting point for evolution consideration is the classical Hamiltonian of the model, expressed in formulas (1)–(3). We recast it in terms of the dimensionless particle number density η and the phase θ for the macroscopic wave function as follows:

$$H = \frac{1}{2} \int_0^{\xi_B} \left[(\partial_\xi \sqrt{\eta})^2 + \eta (\partial_\xi \theta)^2 + \frac{A}{2} \eta \Delta_\xi^{-1} \eta + 2(1 - \cos \sqrt{\eta}) - \eta \right] \xi^2 d\xi. \quad (129)$$

This generates the Hamiltonian equations, that is, the BEC hydrodynamic equations:

$$\partial_\tau \theta(\xi, \tau) = -\frac{\delta H}{\delta \eta(\xi, \tau)}, \quad \partial_\tau \eta(\xi, \tau) = \frac{\delta H}{\delta \theta(\xi, \tau)}. \quad (130)$$

Substituting $\eta(\xi, \tau) \rightarrow \eta(\xi) + \delta\eta(\xi, \tau)$ and $\theta(\xi, \tau) \rightarrow -u\tau + \theta(\xi, \tau)$, we extract from H the contribution quadratic in the perturbations $\delta\eta$ and θ – the second variation:

$$H^{(2)} = \frac{1}{2} \int_0^{\xi_B} \left[-\frac{\delta\eta}{4} \tilde{\Delta}_\xi \frac{\delta\eta}{\eta} - \eta \theta \tilde{\Delta}_\xi \theta + \frac{A}{2} \delta\eta \Delta_\xi^{-1} \delta\eta + \frac{c_s^2}{2\eta} (\delta\eta)^2 \right] \xi^2 d\xi. \quad (131)$$

The first term of quantum fluctuations follows from the direct expansion of $(\partial_\xi \sqrt{\eta + \delta\eta})^2$ up to the order $(\delta\eta)^2$ and integration by parts.

Taking into account the equations of motion, equal to (86) without a baryon source,

$$\left(c_s^2 - \frac{\tilde{\Delta}_\xi}{2} \right) \frac{\delta\eta}{\eta} + A \Delta_\xi^{-1} \delta\eta = 2\partial_\tau \theta, \quad -\eta \tilde{\Delta}_\xi \theta = \partial_\tau \delta\eta, \quad (132)$$

one has

$$H^{(2)} = \frac{1}{2} \int_0^{\xi_B} (\theta \partial_\tau \delta \eta - \delta \eta \partial_\tau \theta) \xi^2 d\xi. \quad (133)$$

Upon substituting the quantized perturbations $\widehat{\delta \eta}$ and $\widehat{\theta}$, and invoking the orthogonality of $\{\varphi_n\}$ and $\{B_{n,m}\}$ as given in (114) and (120), we formally obtain the canonical quantum Hamiltonian:

$$\widehat{H}^{(2)} = \frac{1}{2} \sum_n \omega_n (\widehat{\beta}_n \widehat{\beta}_n^\dagger + \widehat{\beta}_n^\dagger \widehat{\beta}_n) = \sum_n \omega_n \left(\widehat{\beta}_n^\dagger \widehat{\beta}_n + \frac{1}{2} \right). \quad (134)$$

Despite its formal resemblance to the Bogolyubov Hamiltonian for excitations, their spectrum $\omega_n = \omega(\kappa_n)$ exhibits distinctive features. In particular, it does not generate phonon modes at small κ , which allows it to be interpreted rather as a single-particle spectrum in the medium. In essence, for $\alpha(\kappa) < 0$ as before, it is governed by the dispersion relation

$$\omega(\kappa) \simeq \frac{1}{2} (\kappa^2 + \alpha(\kappa)), \quad \kappa \gg 1. \quad (135)$$

At small κ , the modes cannot even be associated with quasiparticles when tunneling through the V_L barrier, as shown in figure 8.

Moreover, the lowest two modes contribute purely imaginary terms into $\widehat{H}^{(2)}$:

$$\widehat{H}^{(2)} = \widehat{H}_0 - i\widehat{\Gamma}_0, \quad (136)$$

$$\widehat{H}_0 = \sum_{n \geq 2} \omega_n \left(\widehat{\beta}_n^\dagger \widehat{\beta}_n + \frac{1}{2} \right), \quad \widehat{\Gamma}_0 = \sum_{n=0,1} |\omega_n| \left(\widehat{\beta}_n^\dagger \widehat{\beta}_n + \frac{1}{2} \right), \quad [\widehat{H}_0, \widehat{\Gamma}_0] = 0. \quad (137)$$

The minus sign preceding $\widehat{\Gamma}_0$ is introduced to ensure that Hamiltonian (134) is recovered under the following identification $|\omega_n| = i\omega_n$, where $i = \sqrt{-1}$ as usual.

While \widehat{H}_0 acts naturally on the Fock space spanned by the occupation number basis, the state space for $\widehat{\Gamma}_0$ is not a simple Fock one [76, 77]. The specific eigenstates of $\widehat{\Gamma}_0$, defined in [77], allow us to retain the Hamiltonian structure and notations in the presence of purely imaginary modes $n = 0, 1$. We also stress the projection method developed in [75] for the BEC with unstable modes.

Thus, the steady BEC background $\eta(\xi)$ for $\xi \in [0; \xi_B]$, where ξ_B is smaller than the Jeans radius, gives rise to two discrete long-wavelength modes with imaginary energies. This spectrum reflects a metastable configuration reminiscent of a false vacuum [78–80]: locally stable but unstable to large-scale perturbations. Although the two unstable modes can be eliminated from the density and conjugate phase perturbations, the quantum energy expression should retain a residual vacuum contribution.

By setting $\widehat{\beta}_n^\dagger = 0$ and $\widehat{\beta}_n = 0$ at $n = 0, 1$, the vacuum contribution enters as a constant

$$\gamma = \frac{1}{2} \sum_{n=0,1} |\omega_n|, \quad (138)$$

which represents the vacuum imprint of this sector.

Due to commutativity of the components, the resulting evolution operator factorizes as

$$e^{-i\widehat{H}_0\tau} e^{-\gamma\tau} \quad \text{for } \tau \geq 0, \quad (139)$$

where the first factor governs the unitary dynamics of the stable quasiparticle modes, while the second factor encodes a universal exponential damping. This structure reflects the intrinsic instability of the quasiparticle vacuum: even excitations in the stable sector decay in time due to the background instability. However, taking into account the specifics of the system, the dependence of the modes on time remains the same as in expressions (124) and (126).

Note that the unstable modes is not invariant under time reversal, $\tau \rightarrow -\tau$. Their manifestation in non-inertial reference frames has been analyzed in [81] from the perspective of the

Unruh effect. This connection may be particularly significant given the role of gravity in their formation.

The relaxation rate due to the decay of metastable states is estimated as

$$\gamma = \frac{1}{2} \sum_{n=0,1} \sqrt{-\frac{\Lambda_n}{2}} \simeq 0.25753, \quad t_{\text{vd}} = \frac{t_0}{\gamma} \simeq 3.23 \times 10^7 \text{ yr.} \quad (140)$$

Taking this into account, hydrodynamic perturbations should weaken over time $t \geq t_{\text{vd}}$, bringing the system to a steady state described by equilibrium $\eta(\xi)$ and $\theta = -u\tau$. Besides, t_{vd} is much smaller than the “infinite-time” limit of $\sim 10^9$ yr.

On the other hand, stable quasiparticles can decay into pairs of quasiparticles with lower energies and momenta. This process, governed by the cubic (third-order) variation of the Hamiltonian

$$H^{(3)} = \frac{1}{2} \int_0^{\xi_B} \left[-\frac{\delta\eta}{4} \left(\partial_\xi \frac{\delta\eta}{\eta} \right)^2 + \delta\eta (\partial_\xi \theta)^2 + \left(\frac{d}{d\eta} \frac{c_s^2}{\eta} \right) \frac{(\delta\eta)^3}{6} \right] \xi^2 d\xi, \quad (141)$$

gives rise to Beliaev damping [74, 82–85]. While the original formulation presumes exact conservation of energy and momentum, such conditions are difficult to satisfy in systems with discrete and non-equidistant spectra. Nevertheless, in the presence of a background medium, not all matrix elements of these decay channels should vanish. Their calculation requires two types of integrals:

$$T_{m,n,k} \equiv \int_0^{\xi_B} \varphi_m \varphi_n \varphi_k \frac{\xi^2 d\xi}{\sqrt{\eta}}, \quad S_{m,n,k} \equiv \int_0^{\xi_B} \sqrt{\eta} j_2(\sqrt{\eta}) \varphi_m \varphi_n \varphi_k \xi^2 d\xi, \quad (142)$$

so that

$$\int_0^{\xi_B} \sqrt{\eta} \varphi_m \left(\partial_\xi \frac{\varphi_n}{\sqrt{\eta}} \right) \left(\partial_\xi \frac{\varphi_k}{\sqrt{\eta}} \right) \xi^2 d\xi = \frac{\lambda_m - \lambda_n - \lambda_k}{2} T_{m,n,k}. \quad (143)$$

As a result, high-energy modes acquire a finite lifetime, rendering them metastable. Their decay cascades can amplify long-wavelength excitations and thereby smooth out the perturbation profiles. A detailed study of this issue will be carried out elsewhere.

5 Conclusion

To model a spherically symmetric dark-matter (DM) halo in dwarf galaxies, we adopt a Bose-Einstein condensate (BEC) framework with axionlike interaction [28, 54]. We focus on solutions to the hydrodynamic equations for small perturbations of decoherent BEC DM, induced by gravitational fluctuations from subgalactic baryons.

To preserve spherical symmetry in our calculations, we restrict ourselves to the central galactic region overlapping the stable DM core – an approximation we consider valid for arbitrary galactic geometries. Using spherical shells constructed from the Plummer distribution [55] for gas and stars, we examine three scenarios: (i) expansion of a gaseous shell reminiscent of stellar explosions, (ii) collapse of a shell needed for star formation, and (iii) migration of a stellar cluster toward the galactic center driven by dynamical friction within a gaseous shell. By representing the time evolution of baryon gravitational potentials in the relaxation-time approximation, we preliminarily estimate the timescale of dynamical friction in the adopted cluster geometry, thereby extending the classical Chandrasekhar formula [60]. Adiabatic variations in the gravitational potential of baryon clusters influence DM through tidal forces, though their effect should remain minor in galaxies dominated by DM.

We apply this approach to the dwarf galaxy NGC 2366, using observational data to extract its characteristics [59]. As shown in [28], a nonuniform BEC DM halo in NGC 2366, consisting of dark axions with fitted mass $m \simeq 1.2 \times 10^{-23} \text{ eV} c^{-2}$ and decay constant $f_a \simeq 3.5 \times 10^{19} \text{ eV}$,

admits two phases induced by axionlike interaction: one stable and one unstable, differing in the sign of the squared speed of sound. Although our results indicate central DM density variations of only $10^{-5} - 10^{-2} \%$ and DM wind velocities of just a few meters per second, they raise the question of whether such small perturbations can meaningfully influence star formation. We also find that larger density enhancements are accompanied by lower hydrodynamic velocities, and the perturbation peaks extend to kiloparsec scales. Moreover, DM winds do not fully attenuate even on timescales several times longer than the baryonic relaxation time.

In this regard, we analyzed the effect of small perturbations in BEC DM, induced by the gravitational imprint of cascaded subgalactic baryonic processes separated in space and time. The results can be summarized as follows. The temporal asymptotes of model gravitational potentials – corresponding to stellar collapse, explosion, and migration – are incorporated through perturbation theory in the chemical potential, which governs the final DM distribution in the galaxy under hydrodynamic relaxation. In the absence of viscosity, damping of the flows arises solely from quantum effects.

Elementary excitations in the DM of NGC 2366, mainly interpreted as quasiparticles, are represented by quantized fields of phase and density fluctuations of the order parameter. In hydrodynamics, these free excitations obey the continuity and Euler equations.

Numerical analysis reveals orthogonal modes of the Laplace-operator analogue in the inhomogeneous medium of fixed volume, corresponding to discrete values of the radial wave number κ . Expanding perturbations in this basis establishes the dependence of their energy spectrum ω on κ . The resulting spectrum reduces to a single-particle spectrum in the medium supporting a potential barrier, as the absence of linear behavior at small κ precludes phonons. Notably, the first two modes possess purely imaginary energies, signaling metastability [79].

In the steady BEC DM background with spatial extent below the Jeans radius, these two modes, corresponding to long-wavelength fluctuations beyond the Jeans scale [35], resemble a false vacuum: locally steady yet unstable to large-scale perturbations. Their quantum formulation in a specific Fock space [77] identifies them as bosons, whose vacuum contribution induces decay on a characteristic timescale of 3.2×10^7 years. This decay ensures temporal damping of the evolution operator for the entire system of free quasiparticles. In laboratory BECs, this vacuum contribution may remain negligible due to comparatively long relaxation times, but it can become a significant effect in astrophysics. At higher perturbation order, Beliaev damping arises from quasiparticle decay, introducing an additional quantum relaxation mechanism [74].

Our findings complement the picture of events occurring in DM halos, described within various models [40–46, 86]. Substantial modifications of DM are expected when it interacts with massive structures. Such changes may occur within large galaxies or be driven by external influences from neighboring galaxies and their DM halos, as well as massive black holes. A more complete treatment needs to quantify the contributions of quantum relaxation processes and establish their role in regulating the stability of BEC DM halos.

Acknowledgments

This work is supported by the Ukrainian-Swiss project No. IZURZ2-224868 “Compact star-forming galaxies and their impact on cosmic reionization and cosmology”.

A Surface density

Let us calculate the surface density of a unit mass:

$$\Sigma_0(R, \check{r}, d) = 2 \int_0^\infty \eta_b \left(\sqrt{z^2 + R^2}, \check{r}, d \right) dz. \quad (144)$$

Defining the parameters $a = \check{r}/R$ and $b = d/R$, we first compute the auxiliary elliptic integral of the first kind (see formulas 3.145 in [87]):

$$\begin{aligned} I_1(a, b) &\equiv \int_0^1 \left[\frac{1}{\sqrt{(1-as)^2 + b^2s^2}} - \frac{1}{\sqrt{(1+as)^2 + b^2s^2}} \right] \frac{ds}{\sqrt{1-s^2}} \\ &= \frac{2}{\sqrt{y}} [K(k) - F(x; k)], \end{aligned} \quad (145)$$

which is determined by

$$\begin{aligned} x &= \frac{2\sqrt{y}}{\sqrt{(1+a)^2 + b^2} + \sqrt{(1-a)^2 + b^2}}, \\ k &= \frac{\sqrt{a^2 + b^2 - 1 + y}}{\sqrt{2y}}, \\ y &= \sqrt{[(1+a)^2 + b^2][(1-a)^2 + b^2]}, \end{aligned} \quad (146)$$

where x is the sine of the amplitude, k is the modulus.

The desired function is represented through the derivative of $I_1(a, b)$:

$$\begin{aligned} I_2(a, b) &\equiv -\frac{\partial I_1(a, b)}{b \partial b} \\ &= \frac{1}{\sqrt{y}} \left(\frac{y_b}{y} + 2 \frac{k_b}{k} \right) [K(k) - F(x; k)] + \frac{2}{\sqrt{y}} \frac{x_b}{\sqrt{1-x^2}\sqrt{1-k^2x^2}} \\ &\quad - \frac{2k_b}{k(1-k^2)\sqrt{y}} \left[E(k) - E(x; k) + k^2 \frac{x\sqrt{1-x^2}}{\sqrt{1-k^2x^2}} \right], \end{aligned} \quad (147)$$

where $E(k)$ and $E(x; k)$ are the complete and incomplete elliptic integrals of the second kind; the subscript b for each parameter w from (146) denotes $w_b = b^{-1}\partial_b w$, determined by the derivative with respect to b .

Calculating, we find that

$$x_b = \frac{x}{y^2}(1+a^2+b^2-y), \quad k_b = \frac{1+b^2-a^2}{y^3k}, \quad y_b = 2\frac{1+a^2+b^2}{y}. \quad (148)$$

Combining, we obtain the surface density profile:

$$\Sigma_0(R, \check{r}, d) = \frac{d^2}{\check{r}R^3} I_2 \left(\frac{\check{r}}{R}, \frac{d}{R} \right). \quad (149)$$

This distribution is normalized as

$$\int_0^{2\pi} d\varphi \int_0^\infty \Sigma_0(R, \check{r}, d) R dR = 4\pi. \quad (150)$$

Thus, the dimensional spatial and surface distributions for the spherical layer (cluster) with the total baryon mass M are

$$\rho_M(r, \check{r}, d) = \frac{M}{4\pi} \eta_b(r, \check{r}, d), \quad (151)$$

$$\Sigma_M(R, \check{r}, d) = \frac{M}{4\pi} \Sigma_0(R, \check{r}, d). \quad (152)$$

References

- [1] R.D. Peccei, H.R. Quinn, *CP conservation in the presence of pseudoparticles*, *Phys. Rev. Lett.* **38** (1977) 1440.
- [2] J. Preskill, M.B. Wise, F. Wilczek, *Cosmology of the invisible axion*, *Phys. Lett. B* **120** (1983) 127.
- [3] L. Abbott, P. Sikivie, *A cosmological bound on the invisible axion*, *Phys. Lett. B* **120** (1983) 133.
- [4] M. Dine, W. Fischler, *The not-so-harmless axion*, *Phys. Lett. B* **120** (1983) 137.
- [5] R.L. Davis, *Cosmic axions from cosmic strings*, *Phys. Lett. B* **180** (1986) 225.
- [6] P. Sikivie, Q. Yang, *Bose-Einstein condensation of dark matter axions*, *Phys. Rev. Lett.* **103** (2009) 111301 [arXiv:0901.1106].
- [7] O. Erken, P. Sikivie, H. Tam, Q. Yang, *Cosmic axion thermalization*, *Phys. Rev. D* **85** (2012) 063520 [arXiv:1111.1157].
- [8] S. Davidson, M. Elmer, *Bose-Einstein condensation of the classical axion field in cosmology?* *JCAP* **12** (2013) 034 [arXiv:1307.8024].
- [9] S. Davidson, *Axions: Bose Einstein condensate or classical field?* *Astropart. Phys.* **65** (2015) 101 [arXiv:1405.1139].
- [10] A.H. Guth, M.P. Hertzberg, C. Prescod-Weinstein, *Do dark matter axions form a condensate with long-range correlation?* *Phys. Rev. D* **92**, 103513 (2015) [arXiv:1412.5930].
- [11] J.D. Breit, S. Gupta, A. Zaks, *Cold Bose stars*, *Phys. Lett. B* **140** (1984) 329.
- [12] L.A. Ureña-López, T. Matos, R. Becerril, *Inside oscillatons*, *Class. Quantum Grav.* **19**, 6259 (2002).
- [13] S. Borsanyi et al., *Calculation of the axion mass based on high-temperature lattice quantum chromodynamics*, *Nature* **539** (2016) 69.
- [14] V.B. Klaer, G.D. Moore, *The dark-matter axion mass*, *JCAP* **11** (2017) 049 [arXiv:1708.07521].
- [15] T. Fukuyama, M. Morikawa, T. Tatekawa, *Cosmic structures via Bose-Einstein condensation and its collapse*, *JCAP* **06** (2008) 033 [arXiv:0705.3091].
- [16] M.R. Baldeschi, G.B. Gelmini, R. Ruffini, *On massive fermions and bosons in galactic halos*, *Phys. Lett. B* **122** (1983) 221.
- [17] S.-J. Sin, *Late-time phase transition and the galactic halo as a Bose liquid*, *Phys. Rev. D* **50** (1994) 3650 [arXiv:hep-ph/9409267].
- [18] J.E.D. Marsh, *Axion cosmology*, *Phys. Rep.* **643** (2016) 1 [arXiv:1510.07633].
- [19] L. Hui, J.P. Ostriker, S. Tremaine, E. Witten, *Ultralight scalars as cosmological dark matter*, *Phys. Rev. D* **95** (2017) 043541 [arXiv:1610.08297].
- [20] W.A. Terrano, E.G. Adelberger, C.A. Hagedorn, B.R. Heckel, *Constraints on axionlike dark matter with masses down to 10^{-23} eV/c²*, *Phys. Rev. Lett.* **122** (2019) 231301
- [21] E. Witten, *Large N chiral dynamics*, *Ann. Phys.* **128** (1980) 363.
- [22] E. Braaten, H. Zhang, *Colloquium: The physics of axion stars*, *Rev. Mod. Phys.* **91** (2019) 041002 [arXiv:1810.11473].
- [23] E.W. Kolb, I.I. Tkachev, *Nonlinear axion dynamics and the formation of cosmological pseudosolitons*, *Phys. Rev. D* **49** (1994) 5040 [arXiv:astro-ph/9311037].
- [24] P.H. Chavanis, *Phase transitions between dilute and dense axion stars*, *Phys. Rev. D* **98** (2018) 023009 [arXiv:1710.06268].

- [25] L. Visinelli, S. Baum, J. Redondo, K. Freese, F. Wilczek, *Dilute and dense axion stars*, *Phys. Lett. B* **777** (2018) 64 [arXiv:1710.08910].
- [26] E.D. Schiappacasse, M.P. Hertzberg, *Analysis of dark matter axion clumps with spherical symmetry*, *JCAP* **01** (2018) 037 [arXiv:1710.04729].
- [27] E.C. Nambo, A. Diez-Tejedor, A.A. Roque, Q. Sarbach, *Linear stability of nonrelativistic self-interacting boson stars*, *Phys. Rev. D* **109** (2024) 104011 [arXiv:2402.07998].
- [28] A. Nazarenko, *Macroscopic states in Bose-Einstein condensate dark matter model with axionlike interaction*, *Eur. Phys. J. C* **85** (2025) 1171 [arXiv:2506.23761].
- [29] J.-W. Lee, In-G. Koh, *Galactic halos as boson stars*, *Phys. Rev. D* **53** (1996) 2236 [arXiv:hep-ph/9507385].
- [30] T. Harko, *Bose-Einstein condensation of dark matter solves the core/cusp problem*, *JCAP* **05** (2011) 022 [arXiv:1105.2996].
- [31] M. Craciun, T. Harko, *Testing Bose-Einstein condensate dark matter models with the SPARC galactic rotation curves data*, *Eur. Phys. J. C* **80**, (2020) 735.
- [32] E. Kun, Z. Keresztes, L. Gergely, *Slowly rotating Bose-Einstein condensate compared with the rotation curves of 12 dwarf galaxies*, *Astron. Astrophys.* **633** (2020) A75.
- [33] P.-H. Chavanis, *Growth of perturbations in an expanding universe with Bose-Einstein condensate dark matter*, *Astron. Astrophys.* **537** (2012) A127 [arXiv:1103.2698].
- [34] T. Harko, *Jeans instability and turbulent gravitational collapse of Bose-Einstein condensate dark matter halos*, *Eur. Phys. J. C* **79** (2019) 787.
- [35] P.-H. Chavanis, *Jeans instability of dissipative self-gravitating Bose-Einstein condensates with repulsive or attractive self-interaction: Application to dark matter*, *Universe* **6** (2020) 226.
- [36] E.G.M. Ferreira, *Ultra-light dark matter*, *Astron. Astrophys. Rev.* **29** (2021) 7 [arXiv:2005.03254].
- [37] T. Harko, E.J. Madarassy, *Bose-Einstein condensate dark matter models in the presence of baryonic matter and random confining potentials*, *Eur. Phys. J. C* **82** (2022) 401.
- [38] P.-H. Chavanis, *A review of basic results on the Bose-Einstein condensate dark matter model*, *Front. Astron. Space Sci.* **12** (2025) 1538434.
- [39] D.J.E. Marsh, J. Silk, *A model for halo formation with axion mixed dark matter*, *Mon. Not. R. Astron. Soc.* **437** (2014) 2652.
- [40] M. Schaller, *Effects of baryons on the dark matter distribution in cosmological hydrodynamical simulations*, Doctoral thesis, Durham University (2015).
- [41] J. Schaye et al. *The FLAMINGO project: cosmological hydrodynamical simulations for large-scale structure and galaxy cluster surveys*, *Mon. Not. R. Astron. Soc.* **526** (2023) 4978 [arXiv:2306.04024].
- [42] J.I. Read, G. Gilmore, *Mass loss from dwarf spheroidal galaxies: the origins of shallow dark matter cores and exponential surface brightness profiles*, *Mon. Not. R. Astron. Soc.* **356** (2005) 107 [arXiv:astro-ph/0409565].
- [43] S. Mashchenko, H. Couchman, J. Wadsley, *The removal of cusps from galaxy centres by stellar feedback in the early Universe*, *Nature* **442** (2006) 539.
- [44] T. Goerdt, B. Moore, J.I. Read, J. Stadel, M. Joachim, *Does the Fornax dwarf spheroidal have a central cusp or core?* *Mon. Not. R. Astron. Soc.* **268** (2006) 1073.
- [45] F. Governato, C. Brook, L. Mayer et al. *Bulgeless dwarf galaxies and dark matter cores from supernova-driven outflows*, *Nature* **463** (2010) 203 [arXiv:0911.2237].

- [46] A. Pontzen, F. Governato, *How supernova feedback turns dark matter cusps into cores*, *Mon. Not. R. Astron. Soc.* **421** (2012) 3464 [arXiv:1106.0499].
- [47] A.M. Gavrilik, M.V. Khelashvili, A.V. Nazarenko, *Bose-Einstein condensate dark matter model with three-particle interaction and two-phase structure*, *Phys. Rev. D* **102** (2020) 083510 [arXiv:2007.04832].
- [48] E.W. Kolb, I.I. Tkachev, *Axion miniclusters and Bose stars*, *Phys. Rev. Lett.* **71** (1993) 3051 [arXiv:hep-ph/9303313].
- [49] A.V. Balatsky, B. Fraser, H.S. Røising, *Dark sound: Collective modes of the axionic dark matter condensate*, *Phys. Rev. D* **105** (2022) 023504 [arXiv:2106.03939].
- [50] P. Di Vecchia, G. Veneziano, *Chiral dynamics in the large N limit*, *Nucl. Phys. B* **171** (1980) 253.
- [51] M. Alcubierre, F.S. Guzmán, T. Matos, D. Núñez, L.A. Ureña-López, P. Wiederhold, *Galactic collapse of scalar field dark matter*, *Class. Quant. Grav.* **19** (2002) 5017 [arXiv:gr-qc/0110102].
- [52] G.G. di Cortona, E. Hardy, J.P. Vega, G. Villadoro, *The QCD axion, precisely*, *J. High Energ. Phys.* **01** (2016) 034 [arXiv:1511.02867].
- [53] P.H. Chavanis, *Dissipative self-gravitating Bose-Einstein condensates with arbitrary nonlinearity as a model of dark matter halos*, *Eur. Phys. J. Plus* **132** (2017) 248 [arXiv:1603.06580].
- [54] A.M. Gavrilik, A.V. Nazarenko, *Axionlike dark matter model involving two-phase structure and two-particle composites*, *Phys. Rev. D* **108** (2023) 123030 [arXiv:2309.03290].
- [55] H.C. Plummer, *On the problem of distribution in globular star clusters: (Plate 8.)*, *Mon. Not. R. Astron. Soc.* **71** (1911) 460.
- [56] W. Israel, *Singular hypersurfaces and thin shells in general relativity*, *Nuovo Cimento B* **44** (1966) 1.
- [57] B.G. Elmegreen, C.J. Lada, *Sequential formation of subgroups in OB associations*, *Astrophys. J.* **214** (1977) 725.
- [58] S.J. Chapman, A.S. Bhattal, M.J. Disney, J.A. Turner, A.P. Whitworth, *Star formation in shocked layers*, *Astrophys. Space Sci.* **216** (1994) 317.
- [59] S.-H. Oh, W.J.G. de Blok, F. Walter, E. Brinks, R.C. Kennicutt Jr., *High-resolution dark matter density profiles of THINGS dwarf galaxies: Correcting for noncircular motions*, *Astronom. J.* **136** (2008) 2761 [arXiv:0810.2119].
- [60] S. Chandrasekhar, *Dynamical friction. I. General considerations: the coefficient of dynamical friction*, *Astrophys. J.* **97** (1943) 255C.
- [61] M.A. Ruderman, E.A. Spiegel, *Galactic wakes*, *Astrophys. J.* **165** (1971) 1.
- [62] Y. Rephaeli and E.E. Salpeter, *Flow past a massive object and the gravitational drag*, *Astrophys. J.* **240** (1980) 20.
- [63] E.C. Ostriker, *Dynamical friction in a gaseous medium*, *Astrophys. J.* **513** (1999) 252 [arXiv:astro-ph/9810324].
- [64] S. Tremain, M.D. Weinberg, *Dynamical friction in spherical systems*, *Mon. Not. R. Astron. Soc.* **209** (1984) 729.
- [65] H. Kim, W.-T. Kim, *Nonlinear dynamical friction in a gaseous medium*, *Astrophys. J.* **703** (2009) 1278 [arXiv:0908.1391].
- [66] A.T. Lee, S.W. Stahler, *Dynamical friction in a gas: the supersonic case*, *Astron. Astrophys.* **561** (2014) A84 [arXiv:1311.3445].

- [67] V. Desjacques, A. Nusser, R. Bühler, *Analytic solution to the dynamical friction acting on circularly moving perturbers*, *Astrophys. J.* **928** (2022) 64 [arXiv:2111.07366].
- [68] L. Lancaster, C. Giovanetti, P. Mocz, Y. Kahn, M. Lisanti, D.N. Spergel, *Dynamical friction in a fuzzy dark matter Universe*, *JCAP* **01** (2020) 001 [arXiv:1909.06381].
- [69] R. Buehler, V. Desjacques, *Dynamical friction in fuzzy dark matter: Circular orbits*, *Phys. Rev. D* **107** (2023) 023516 [arXiv:2207.13740].
- [70] H. Koo, J.-W. Lee, *Dynamical friction for circular orbits in self-interacting ultralight dark matter and Fornax globular clusters*, *JCAP* **01** (2026) 020 [arXiv:2504.19219].
- [71] E.V. Gorbar, O.V. Barabash, V.M. Gorkavenko, K. Korshynska, A.I. Momot, A.O. Zaporozhchenko, *Damping of dynamical friction force in self-interacting ultralight dark matter and Fornax timing problem*, arXiv:2511.06123
- [72] L. Berezhiani, B. Elder, J. Khoury, *Dynamical friction in superfluids*, *JCAP* **10** (2019) 074 [arXiv:1905.09297].
- [73] C.L. Martin, R.C. Kennicutt, Jr. *Star formation thresholds in galactic disks*, *Astrophys. J.* **555** (2001) 301 [arXiv:astro-ph/0103181].
- [74] E.M. Lifshitz, L.P. Pitaevskii, *Statistical physics, part 2: Theory of the condensed state*, Pergamon Press, Oxford, England (1980).
- [75] A. Izquierdo, M. Arazo, S. Martinez-Garaot, M. Modugno, *Quasiparticle projection method for dynamically unstable Bose-Einstein condensates*. arXiv:2512.13847
- [76] M. Mine, M. Okumura, T. Sunaga, Y. Yamanaka, *Quantum field theoretical description of unstable behavior of trapped Bose-Einstein condensates with complex eigenvalues of Bogoliubov-de Gennes equations*, *Ann. Phys.* **322** (2007) 2327 [arXiv:cond-mat/0609052].
- [77] K. Kobayashi, M. Mine, M. Okumura, Y. Yamanaka, *Quantum field theoretical analysis on unstable behavior of Bose-Einstein condensates in optical lattices*, *Ann. Phys.* **323** (2008) 1247 [arXiv:0706.0959].
- [78] S. Coleman, *Fate of the false vacuum: Semiclassical theory*, *Phys. Rev. D* **15** (1977) 2929.
- [79] E.V. Shuryak, *Metastable Bose condensate made of atoms with attractive interaction*, *Phys. Rev. A* **54** (1996) 3151.
- [80] C. Yin, F.M. Surace, A. Lucas, *Theory of metastable states in many-body quantum systems*, *Phys. Rev. X* **15** (2025) 011064.
- [81] B.S. Felipe, J.P.M. Pitelli, *Unstable mode and the Unruh-DeWitt detector*, *Phys. Rev. D* **112** (2025) 085027.
- [82] S.T. Beliaev, *Energy-spectrum of a non-ideal Bose gas*, *Sov. Phys. JETP* **7** (1958) 299.
- [83] M. Möttönen, S.M.M. Virtanen, M.M. Salomaa, *Collapse and revival of excitations in Bose-Einstein condensates*. *Phys. Rev. A* **71** (2005) 023604 [arXiv:cond-mat/0502441].
- [84] M.-C. Chung, A.B. Bhattacharjee, *Damping in 2D and 3D dilute Bose gases*, *New J. Phys.* **11** (2009) 123012.
- [85] V. Pastukhov, *Damping of Bogoliubov excitations at finite temperatures*, *J. Phys. A: Math. Theor.* **48** (2015) 405002.
- [86] H. Kim, A.Lenoci, *Gravitational focusing of wave dark matter*, *Phys. Rev. D* **105** (2022) 063032 [arXiv:2112.05718].
- [87] I.S. Gradshteyn, I.M. Ryzhik, *Tables of integrals, series, and products*, Academic Press, New York, USA (2007).